Open access • Posted Content • DOI:10.1101/654616

Identification of 3’ UTR motifs required for mRNA localization to myelin sheaths in vivo

Katie M. Yergert, Rebecca O’Rouke, Jacob H. Hines, Bruce Appel

Institutions: Anschutz Medical Campus, Winona State University

Published on: 11 Aug 2020 - bioRxiv (Cold Spring Harbor Laboratory)

Topics: Oligodendrocyte, Myelin, MRNA transport and Untranslated region

Full title: Identification of 3' UTR motifs required for mRNA localization to myelin sheaths in vivo

Short title: mRNA localization to myelin sheaths

Authors: Katie M. Yergert[1], Rebecca O'Rouke[1], Jacob H. Hines[2] and Bruce Appel[1]

[1] Department of Pediatrics, University of Colorado Anschutz Medical Campus, Aurora, Colorado, 80045, USA

[2] current address: Department of Biology, Winona State University, Winona, Minnesota, 55987, USA

ABSTRACT

Myelin is a specialized membrane produced by oligodendrocytes that insulates and supports axons. Oligodendrocytes extend numerous cellular processes, as projections of the plasma membrane, and simultaneously wrap multiple layers of myelin membrane around target axons. Notably, myelin sheaths originating from the same oligodendrocyte are variable in size, suggesting local mechanisms regulate myelin sheath growth. Purified myelin contains ribosomes and hundreds of mRNAs, supporting a model that mRNA localization and local protein synthesis regulate sheath growth and maturation. However, the mechanisms by which mRNAs are selectively enriched in myelin sheaths are unclear. To investigate how mRNAs are targeted to myelin sheaths, we tested the hypothesis that transcripts are selected for myelin enrichment through consensus sequences in the 3' untranslated region (3' UTR). Using methods to visualize mRNA in living zebrafish larvae, we identified candidate 3' UTRs that were sufficient to localize mRNA to sheaths and enriched near growth zones of nascent membrane. We bioinformatically identified motifs common in 3' UTRs from three myelin-enriched transcripts and determined that these motifs are required for mRNA transport to myelin sheaths. Finally, we show that one motif is highly enriched in the myelin transcriptome, suggesting that this sequence is a global regulator of mRNA localization during developmental myelination.

INTRODUCTION

In the central nervous system, myelin provides metabolic support and increases conduction velocity along axons. Myelin is produced by oligodendrocytes, glial cells that extend multiple long processes and wrap layers of membrane around axons. Myelin sheaths originating from a single oligodendrocyte can vary considerably in length and thickness, suggesting that sheath growth is locally regulated (1–3). In line with this model, the myelin transcriptome is distinct compared to the cell body (4). For example, proteolipid protein (PLP) and myelin basic protein (MBP) are the most abundant proteins in myelin. Yet the underlying mechanisms driving their protein expression in the myelin are entirely different. *Plp* mRNA is retained in the cell body and translated at the endoplasmic reticulum and the protein is transported to myelin (5,6). By contrast, *Mbp* mRNA is trafficked to nascent sheaths and locally translated (5–10). This evidence supports the model that mRNAs are selectively targeted to nascent sheaths and locally translated during growth and maturation.

Transport and local translation of mRNAs are broadly utilized mechanisms for controlling subcellular gene expression. In neurons, mRNAs are subcellularly localized to axons (11–13), dendrites (14) and growth cones (15) and local translation is required for axon growth and synaptogenesis (16–19). Frequently, mRNA localization in neurons is determined by elements within the 3' UTR (20,21). For instance, the 3' UTR of *β-actin* contains a sequence that is recognized by the RNA binding protein ZBP1 for localization to cellular projections including growth cones, axons and dendrites (22–26). Neurons localize hundreds of mRNAs to different subcellular compartments but the underlying localization elements within the transcripts are largely unknown.

Similar to neurons, oligodendrocytes localize hundreds of mRNAs to distal myelin sheaths (27), but the localization signals necessary for myelin enrichment are limited to a few mRNAs. To date, the most extensively investigated transcript in oligodendrocytes is *Mbp* mRNA. The *Mbp* 3' UTR is required for mRNA localization to myelin sheaths (28,29) and contains two minimal sequences including a 21-nt conserved sequence that is necessary for localization to processes in cultured mouse

oligodendrocytes (30,31). However, the minimal sequence is not required for localization in vivo, indicating that the *Mbp* 3' UTR contains clandestine localization signals (29). The investigations into *Mbp* mRNA localization have provided significant insights into the molecular mechanisms underlying mRNA localization in oligodendrocytes. However, we know very little about the mechanisms that promote localization of the other hundreds of myelin transcripts. How are mRNAs selected for localization to myelin sheaths? Do myelin-localized transcripts share similar cis-regulatory elements?

Here we bioinformatically identified myelin-enriched transcripts and investigated the ability of their 3' UTR sequences to promote mRNA localization to nascent sheaths in living zebrafish. The 3' UTRs that promote myelin localization contain shared cis-regulatory motifs necessary for mRNA localization. In particular, we identified a sequence motif that is highly enriched in the myelin transcriptome, implicating it as a global regulator of mRNA localization in myelinating oligodendrocytes. Together, our data support a model whereby motifs in 3' UTRs promote mRNA localization to nascent myelin sheaths.

RESULTS

Quantification of mRNA within myelin sheaths of live zebrafish larvae

Although some transcripts, including *Mbp* and *Mobp* mRNA, are present in myelin (7–9,27,32) we lack information about the precise spatial distribution of myelin-enriched mRNAs in vivo. We therefore adapted the MS2 system (33) to visualize and quantify mRNA in myelinating oligodendrocytes of living zebrafish larvae. The MS2 system consists of a mRNA containing a *24xMBS* (MS2 binding sites) sequence, which forms repetitive stem loops, and MCP-EGFP (MS2 coat protein), a reporter protein that specifically binds the *24xMBS* stem loops for visualization of the mRNA via EGFP (Figure 1A). A nuclear localization signal is fused to the MCP-EGFP sequestering unbound MCP-EGFP in the nucleus thus reducing background fluorescence. To drive expression of MCP-EGFP in oligodendrocyte lineage

cells, we created an expression plasmid, *sox10:NLS-tdMCP-EGFP*. Next we created *mbpa:mScarlet-Caax-24xMBS-3'UTR* to drive expression of mRNAs with various 3' UTR elements in myelinating oligodendrocytes (Figure 1A). Additionally, this plasmid also encodes expression of mScarlet-Caax, which acts as a myelin membrane reporter.

As proof of principle, we first tested the 3' UTR of *mbpa*, a zebrafish ortholog of *Mbp*, which promotes mRNA localization in myelin (29). As a control, we used the *sv40* polyadenylation signal, which lacks any known localization signals (34,35) (Figure 1B). To examine mRNA localization in individual oligodendrocytes, we transiently expressed *sox10:NLS-tdMCP-EGFP* with either *mbpa:mScarlet-Caax-24xMBS-mbpa 3'UTR* or *mbpa:mScarlet-Caax-24xMBS-sv40 3'UTR* by microinjection into 1-cell stage zebrafish embryos. This approach revealed mRNA, via EGFP fluorescence intensity, in the cytoplasm of nascent sheaths at 4 days post fertilization (dpf). Consistent with previous reports, we found that the *mbpa* 3' UTR was sufficient to localize mRNA to nascent sheaths in vivo (Figure 1C,D). Furthermore, this approach demonstrated active translation of the *mScarlet-Caax* reporter mRNA. We also observed differences in the mScarlet-Caax fluorescence intensity, at the protein level, between the *sv40* and *mbpa* 3' UTR constructs which could be explained by 3' UTR-mediated difference in translation efficiency (Figure 1C,D).

To quantify mRNA abundance, we measured the average fluorescence intensity of EGFP in myelin sheaths. Due to high levels of fluorescent signal emitting from the cell body, we measured small regions (7 μm) of myelin sheaths far from the cell body. We found that the average fluorescence intensity of sheaths expressing the *mbpa* 3' UTR were approximately two-fold greater than the control (Figure 1E). Importantly, the difference in mRNA localization to myelin sheaths was not due to variability in expression levels of the MS2 reporter (Figure 1F). To verify that cytoplasmic fluorescence is mediated through the mRNA, we removed the *24xMBS* and found that EGFP was retained in the nucleus throughout developmental myelination (Fig 1G,H). Together, these experiments confirm the ability to visualize and quantify mRNA localization during developmental myelination in vivo.

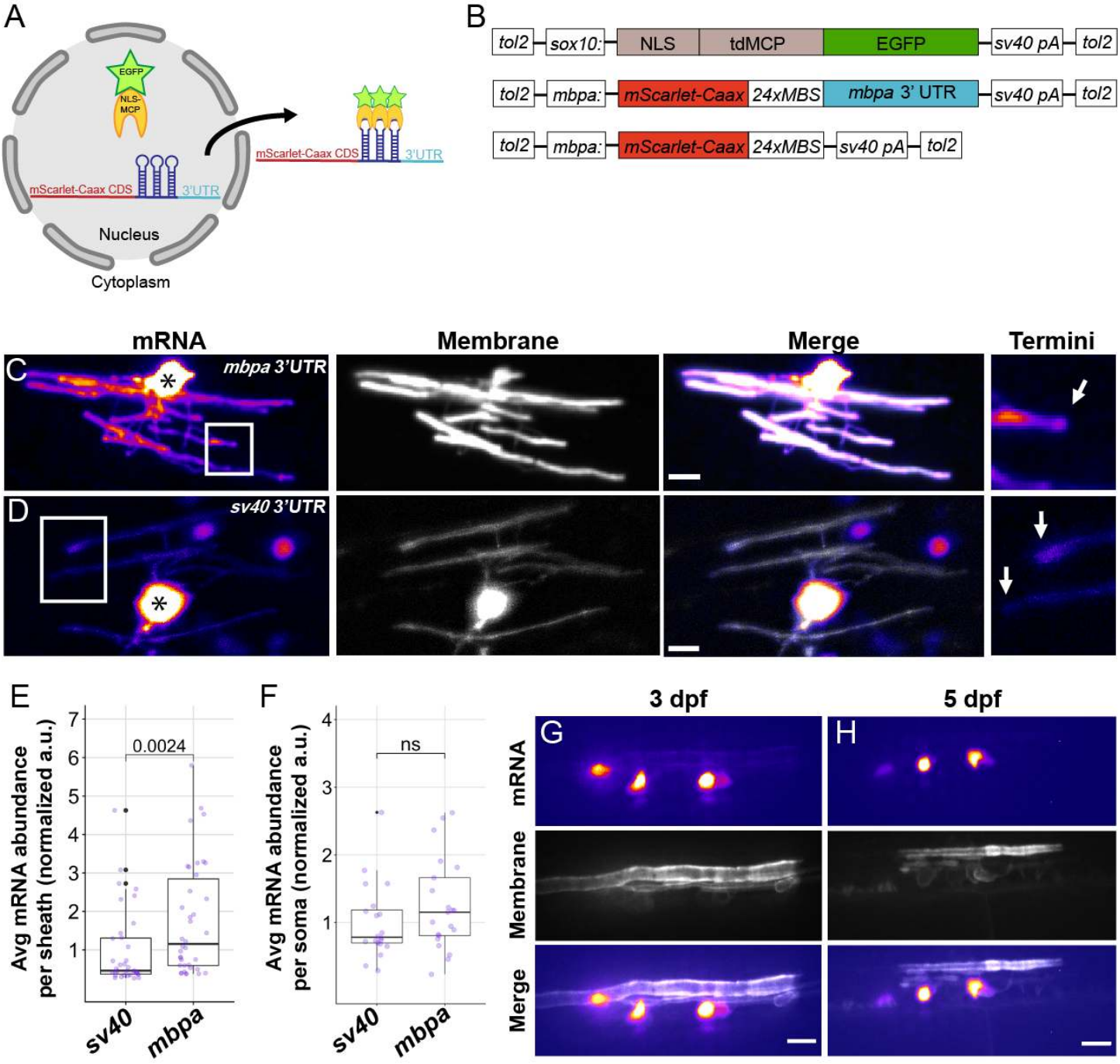

Figure 1. The *mbpa* 3'UTR is sufficient to localize mRNA to myelin sheaths in living zebrafish

(A) Schematic of the MS2 system to visualize mRNA localization in oligodendrocytes. *sox10* regulatory DNA drives expression of nuclear-localized MS2 coat protein, NLS-MCP-EGFP (orange crescent and green star). *mbpa* regulatory elements drive expression of mRNA encoding mScarlet-CAAX fluorescent protein with a repetitive sequence that creates 24 stem loops (24xMBS). When co-expressed, the mRNA-protein complex is exported from the nucleus and localized via the 3' UTR. (B) Schematic of MS2 expression plasmids used for

transient expression in oligodendrocytes with target sequences for Tol2 transposase to facilitate transgene integration. (C-D) Representative images of localization directed by the *mbpa* (C) or control *sv40* 3' UTR (D). Asterisks mark cell bodies with high expression levels of the nuclear localized MCP-EGFP. Boxed areas are enlarged to highlight sheath termini (arrows). (E) Average mRNA abundance per myelin sheath, measured by EGFP fluorescence intensity normalized to the average intensity of the *sv40* control. *sv40*: n= 5 larvae, 35 sheaths. *mbpa*: n= 6 larvae, 38 sheaths. (F) Average mRNA abundance per soma, measured by EGFP fluorescence intensity normalized to the average intensity of the *sv40* control. *sv40*: n= 11 larvae, 20 cell bodies. *mbpa*: n= 15 larvae, 21 cell bodies. (G-H) Representative images of two myelinating oligodendrocytes expressing mRNA lacking the *24xMBS*. NLS-MCP-EGFP remains in the nucleus at 3 dpf (G) and 5 dpf (H). Scale bars, 10 μm. Statistical significance evaluated using Wilcoxon test.

***mbpa* mRNA localizes to the leading edge of developing myelin sheaths**

Previously, *mbpa* transcripts have been detected in sheaths throughout developmental myelination (29,36,37) but the proportion of mRNA that is transported to myelin sheaths is unknown. To quantify the distribution of endogenous *mbpa* mRNA localization in cell bodies and myelin sheaths, we performed single molecule fluorescent in situ hybridization (smFISH) on *Tg(mbpa:egfp-caax)* larvae, which express membrane-tethered EGFP-CAAX in the myelin tracts of the larval hindbrain (Figure 2A). As a control, we also detected *egfp* mRNA encoded by the transgene, which does not contain any known mRNA localization signals (Figure 2B). To quantify mRNA abundance, we calculated the average integrated density of each transcript in both oligodendrocyte cell bodies and in comparable volumes of myelin in the hindbrain. *mbpa* mRNA abundance in myelin sheaths significantly increased between 3 and 4 dpf before reaching a plateau at 5 dpf (Figure 2C), indicating that the majority of *mbpa* mRNA is transported to myelin sheaths at 4 dpf. Specifically, we found that 37% of *mbpa* transcripts localized to myelin sheaths at 4 dpf, whereas only 4% of the *egfp* transcripts localized to the myelin (Figure 2D). We therefore performed all subsequent experiments at 4 dpf, during the peak of active *mbpa* mRNA transport.

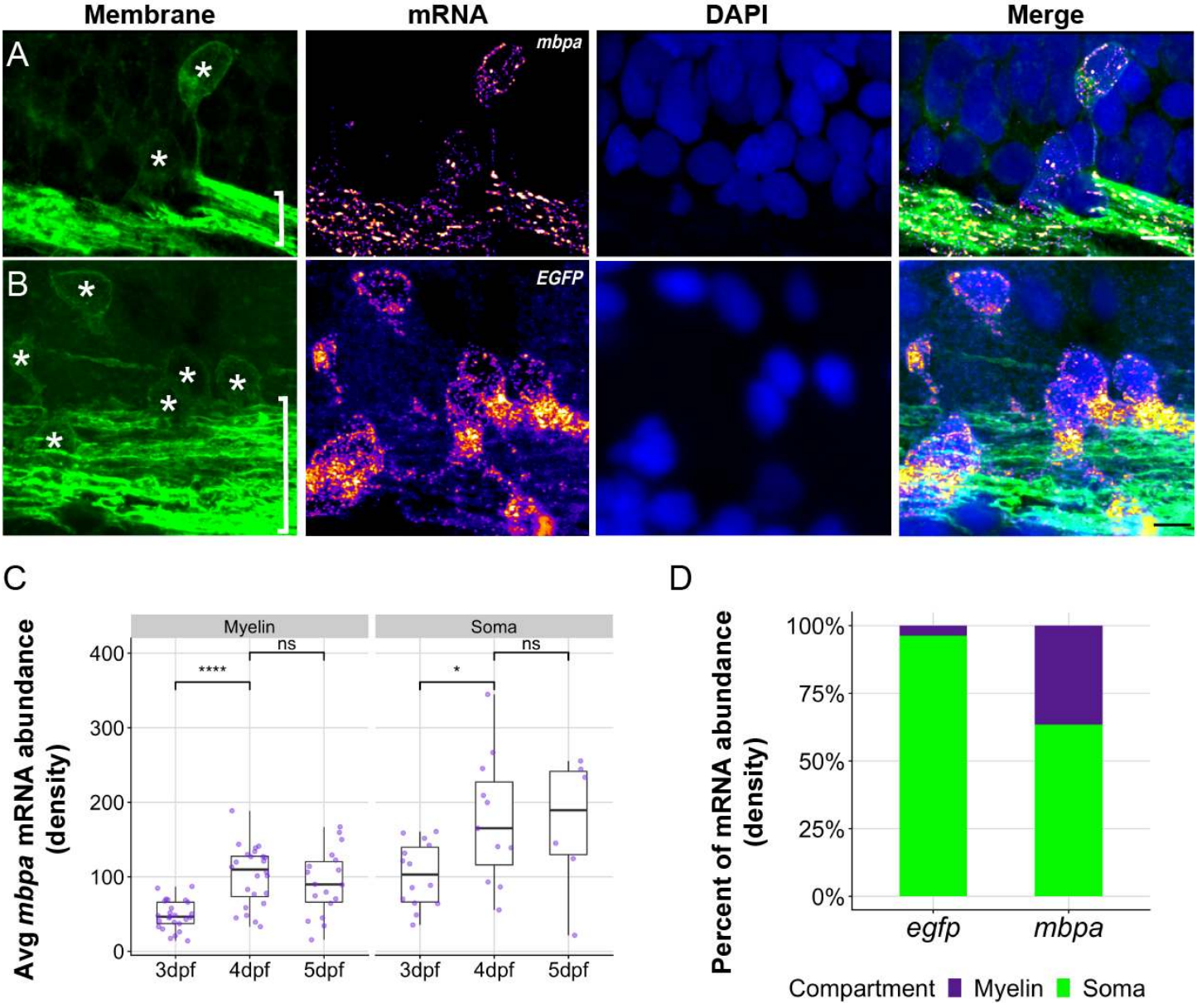

Figure 2. Endogenous *mbpa* mRNA localizes to myelin sheaths between 3-5 dpf

(A-B) Representative images of smFISH experiments using 4 dpf transgenic larva expressing EGFP-CAAX to mark oligodendrocytes. Images show sagittal sections of the hindbrain. DAPI stain labels nuclei. Sections were treated with smFISH probes designed to detect *mbpa* (A) or *egfp* (B) mRNA. Asterisks mark cell bodies and brackets mark myelin tracts. Scale bars, 10 μm. (C) Average *mbpa* mRNA density per cell body or equivalent volume of myelin from 3 to 5 dpf. Density was measured using the integrated density of fluorescence intensity in cell bodies and approximately equal volumes of myelin along the myelin tracts. A minimum (n) for each group was 3 larvae, 6 cell bodies and 15 myelin regions. Statistical significance evaluated using Wilcoxon test. (D)

Proportion of *egfp* or *mbpa* mRNA abundance in cell bodies compared to myelin tracts. A minimum (n) for each group was 3 larvae, 11 cell bodies and 21 myelin regions.

The improved spatial resolution of our smFISH and MS2 approaches allowed us to examine subsheath localization of mRNA within nascent sheaths. We therefore examined the distribution of single *mbpa* transcripts from both longitudinal (Figure 3A,B) and transverse (Figure 3C) orientations using smFISH. This revealed transcripts as discrete puncta distributed along the length of individual sheaths (Figure 3A) and at sheath termini (Figure 3B), consistent with live-imaging observations using the MS2 system (Figure 1C). This distribution was reminiscent of filamentous actin (F-actin) at the leading edge of myelin sheaths (38–40). To determine if mRNA is localized at the leading edge of myelin membrane during wrapping, we co-expressed the MS2 system and Lifeact-mNeonGreen, a F-actin reporter. We found that transcripts containing the *mbpa* 3' UTR colocalized with F-actin (Figure 3D) indicating that mRNA occupies the leading edge of myelin sheaths.

To determine the frequency at which mRNA localizes to the leading edge we used the MS2 system to quantify the number of sheath termini that are enriched with mRNA. We found that 47% of sheath termini have *mbpa* 3' UTR-containing mRNA in comparison to 27% of the *sv40* 3' UTR control (Figure 3E). To precisely define the spatial organization of mRNA at sheath termini, we measured the fluorescence intensity of the MS2 mRNA reporter system across a 7 μm distance at the ends of each sheath. We found that mRNA containing the *mbpa* 3' UTR was significantly enriched within 2 microns of the terminal end (Figure 3F). However, mRNA containing the *sv40* 3' UTR was uniformly distributed along the length of the sheath and lacked enrichment at the leading edge (Figure 1D and 3E). Our data support the conclusion that the *mbpa* 3' UTR is sufficient to localize mRNA to the leading edge of nascent sheaths during developmental myelination.

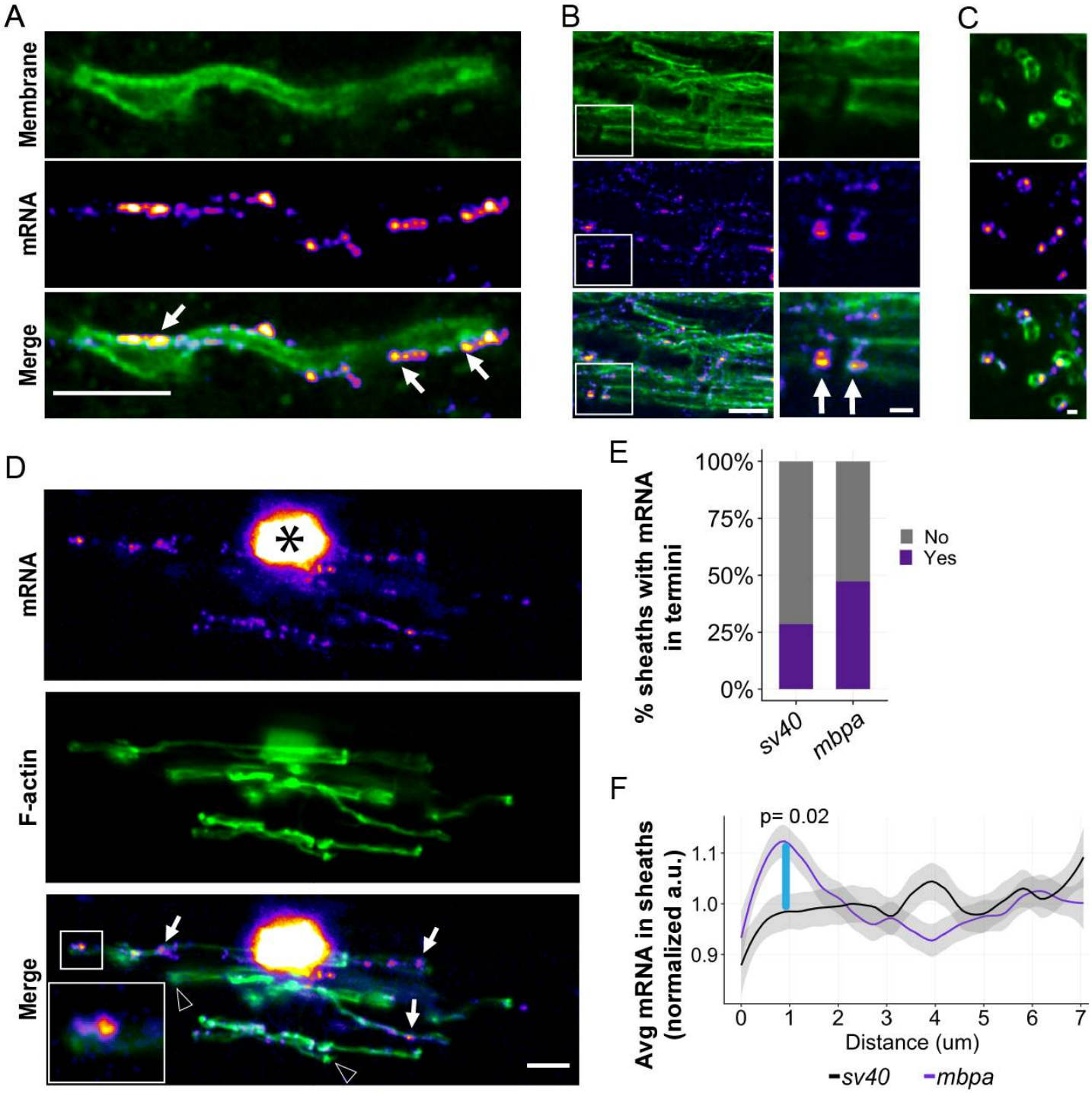

Figure 3. The *mbpa* 3'UTR is sufficient to localize mRNA to the leading edge of myelin sheaths during wrapping

(A) smFISH images of a single optical section of a myelin sheath in a 3 dpf larva spinal cord. *mbpa* transcripts line the myelin sheath. Arrows highlight clusters of *mbpa* mRNA transcripts. (B) smFISH images of a single optical section of myelin tracts in the hindbrain of a 5 dpf larva. Boxed area magnified to highlight sheath termini (arrows). (C) smFISH images of a single optical section in transverse plane of myelin sheaths in a 5 dpf larva midbrain. Scale bars (A-B, D), 5 μm; (C, boxed enlargements), 1 μm. (D) Representative images from MS2 system showing colocalization of mRNA containing *mbpa* 3' UTR and F-actin in a myelinating oligodendrocyte. Asterisk marks the cell body and boxes are magnified to highlight sheath termini. Arrows highlight sheaths with mRNA and arrowheads highlight sheaths lacking mRNA. (E) Proportion of sheaths with mRNA enriched in sheath termini at 4 dpf using the MS2 system. Proportion measured as (sheaths with enrichment / number of sheaths) = 10/35 *sv40,* 18/38 *mbpa*. (F) Average fluorescence intensity of MS2 mRNA reporter containing the *sv40* or *mbpa* 3' UTRs across a 7 μm distance, at 0.2 μm intervals, from myelin sheath termini at 4 dpf. Each line scan was normalized to the average fluorescent intensity per sheath. All normalized values for each distance were then averaged. Shaded area represents 95% confidence interval. Statistical significance was evaluated every 0.2 μm using Wilcoxon test and the distance between 0.8-1.0 μm was statistically significant (blue line). *sv40* 3' UTR n= 5 larvae, 35 sheaths. *mbpa* 3' UTR n= 6 larvae, 38 sheaths.

mRNA localization to myelin sheaths is determined by unique 3' UTR motifs

Our data corroborates previous work demonstrating the sufficiency of the *Mbp* 3' UTR in mRNA localization to myelin. Do other myelin-localized transcripts utilize 3' UTR-dependent mechanisms for localization? To investigate this question, we bioinformatically identified six candidate 3' UTRs from myelin-localized transcripts (Figure 4A). Specifically, we selected candidate 3' UTRs by filtering RNA sequencing data obtained from purified myelin isolated from P18 mouse brain (27) for the gene ontology (GO) terms oligodendrocyte, myelin, translation and synapse. We used the latter two terms because we are interested in the possibility that features of myelin plasticity are similar to synaptic plasticity (41). We narrowed the candidate genes by expression levels in oligodendrocyte lineage cells from published RNA-seq datasets (42,43), descriptions of gene functions from literature searches, and identification of

zebrafish orthologs. This pipeline identified six candidate genes for which we cloned the 3' UTR sequences: *cadm1b*, *cyfip1*, *dlg1*, *eif4ebp2*, *fmr1* and *lrrtm1* (Figure 4C).

Using the MS2 system, we found that inclusion of 3' UTRs from our candidate genes led to a wide variation in mRNA localization to nascent sheaths. Strikingly, the 3' UTRs from *eif4ebp2*, *fmr1* and *lrrtm1* produced significantly greater levels of fluorescence intensities in myelin sheaths than the *sv40* control whereas the remainder, *cadm1b*, *cyfip1*, and *dlg1* were similar to the *sv40* control (Figure 4B,D). Given that all six candidate transcripts are found in purified myelin, our data suggest that only a subset of myelin transcripts are localized by their 3' UTRs and other transcripts likely utilize cis-regulatory elements not present in the 3' UTR or, alternatively, are passively localized to myelin. Nonetheless, these data expand the repertoire of 3' UTR-dependent mRNA localization to myelin sheaths in vivo.

To validate the MS2 findings, we confirmed that endogenous transcripts of *eif4ebp2* and *fmr1* are expressed by oligodendrocytes and are localized to myelin. We chose these transcripts because the 3' UTRs are highly enriched in nascent sheaths (Figure 4D) and they encode translational regulators that are necessary for proper myelination (44) and cognition (45–47). To investigate the spatiotemporal expression of endogenous *fmr1* and *eif4ebp2* transcripts, we used smFISH on *Tg(mbpa:egfp-caax)* larvae to label oligodendrocyte cell bodies and myelin tracts during developmental myelination. In line with the MS2 data, we observed endogenous *fmr1* expression in the cell bodies and myelin sheaths between 4-5 dpf (Figure 5A-D). In contrast, *eif4ebp2* had minimal expression in oligodendrocytes at 4 dpf (Figure 5A) but was prominent in both cell bodies and myelin sheaths by 5 dpf (Figure 5C,D). Together our data show that *fmr1* and *eif4ebp2* transcripts are localized to myelin sheaths, at least in part, by 3' UTRs.

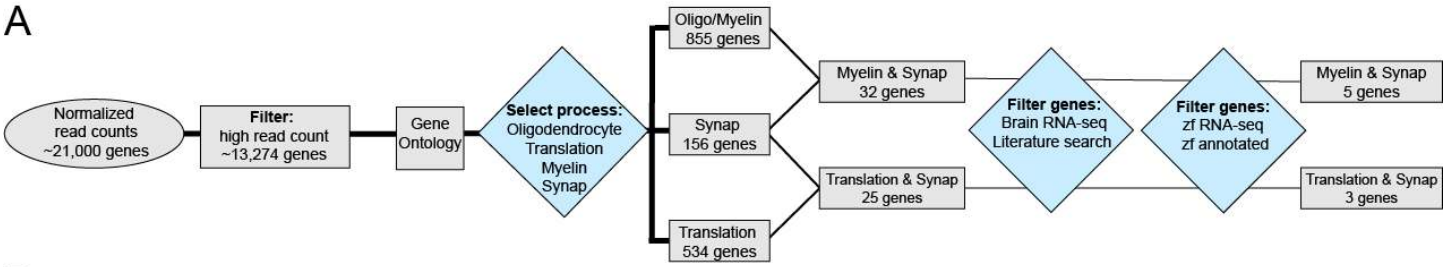

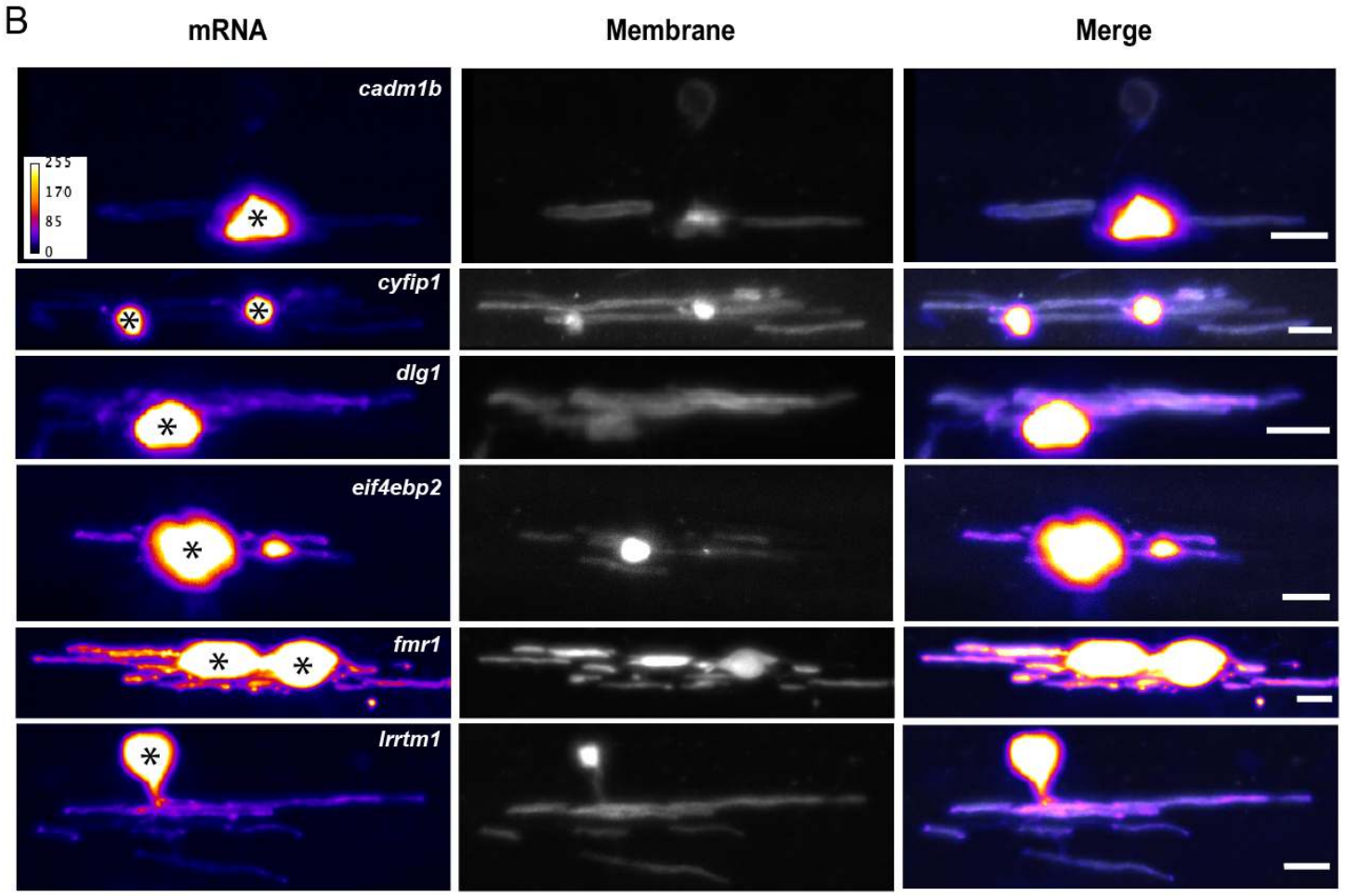

C

Candidate 3'UTRs		
Gene name	Length (nt)	% of 3' UTR
cadm1b	1220	100%
cyfip1	858	88.1%
dlg1	1522	97.2%
eif4ebp2	2282	98.5%
fmr1	2486	99.4%
lrrtm1	368	93.6%

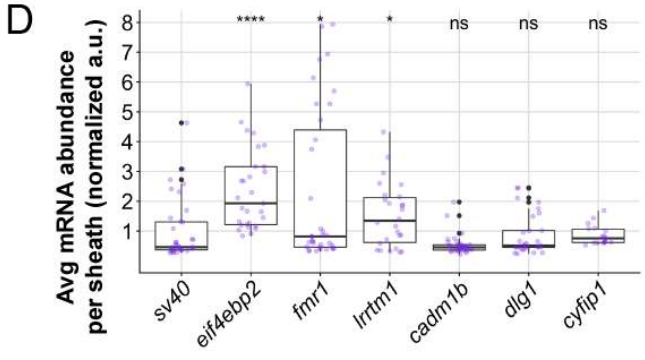

Figure 4. Different 3' UTRs have distinct effects on mRNA localization to myelin sheaths

(A) Work flow to identify 3' UTR candidates from RNA-seq data (27,42,43). (B) Representative images from MS2 system showing localization of mRNAs containing different 3' UTR sequences in oligodendrocytes. Asterisks

mark cell bodies. Scale bars, 10 μm. (C) Table listing candidate 3' UTRs incorporated into the MS2 system, 3' UTR length and the percentage of sequence that was cloned based on the annotated genome. (D) Average mRNA abundance, measured by average EGFP fluorescent intensity, per myelin sheath for each 3' UTR. Normalized to *sv40* control, statistical significance evaluated using Wilcoxon test. A minimum (n) of 5 larvae and 18 sheaths were used in each condition at 4 dpf.

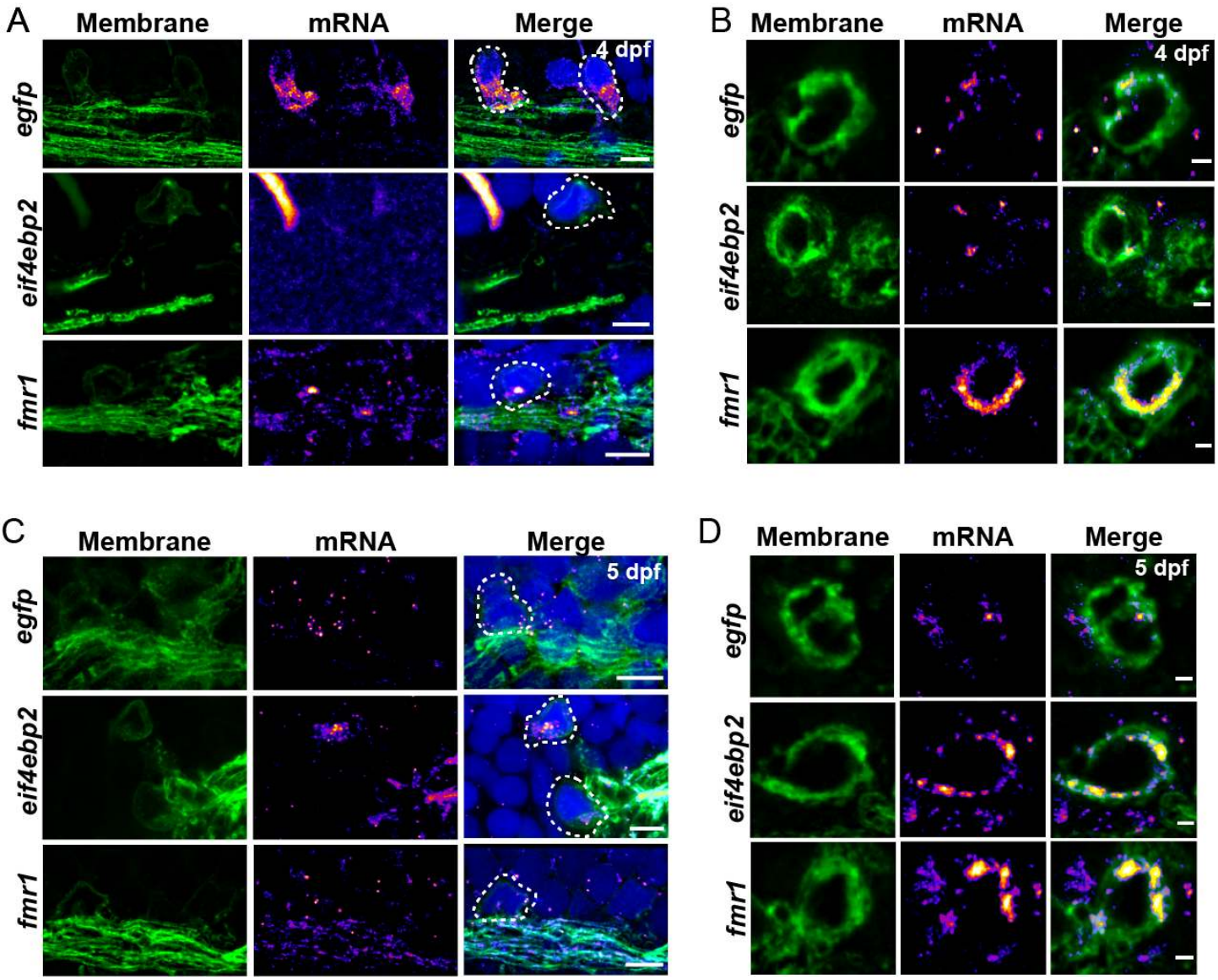

Figure 5. *eif4ebp2* and *fmr1* mRNA are localized to sheaths during developmental myelination

Representative images of smFISH experiments to visualize *egfp*, *eif4ebp2*, or *fmr1* mRNA localization at 4 dpf (A-B) and 5 dpf (C-D) in sagittal sections of hindbrain (A,C) or transverse sections of the Mauthner axon in the

spinal cord (B,D). Dashed lines outline cell bodies marked by EGFP-CAAX. Scale bars, 5 μm (A,C) or 1 μm (B,D).

Localized 3' UTRs share sequence motifs that are required for mRNA localization

3' UTRs frequently contain regulatory elements necessary for post-transcriptional regulation including subcellular localization (20,21). Therefore, we hypothesized that the candidate 3' UTRs share cis-regulatory elements that promote localization to myelin. To test this hypothesis, we used MEME suite bioinformatics software (48,49) to identify shared motifs amongst the *mbpa*, *eif4ebp2*, and *fmr1* 3' UTRs from the annotated zebrafish genome. We identified 3 motifs shared between the candidate 3' UTRs (Figure 6A). However, the *mbpa* 3' UTR we isolated from zebrafish cDNA is truncated by 118 nucleotides at the 3' end and does not contain motif 1. Additionally, the *mbpa* 3' UTR contains a previously identified, conserved RNA transport signal (RTS) (29,50). However, motif 2 and 3 do not overlap with the RTS element suggesting these motifs are novel localization elements (Figure 6B). Importantly, the identified motifs were absent from the non-enriched 3' UTRs (*cadm1b*, *cyfip1*, and *dlg1*) and the *lrrtm1* 3' UTR. To test requirements for these motifs, we deleted all the sequences corresponding to the identified motifs from each 3' UTR and examined mRNA localization using the MS2 system. We found that deletion of all motifs restricted mRNA to the cell bodies (Figure 6C,D). To narrow down which of the motifs are required for localization, we individually deleted each motif and found that removal of any motif reduced mRNA localization in myelin (Figure 6E). Moreover, deletion of motif 1 from the *eif4ebp2* 3' UTR reduced mRNA localization further than the control.

We next tested whether the shared motifs are sufficient to localize mRNA to myelin sheaths. We cloned the motifs from each candidate 3' UTR upstream of the sv40 polyadenylation signal (Figure 7A) and examined mRNA expression in oligodendrocytes using the MS2 system. We found that insertion of *mbpa*-derived sequence motifs were sufficient to localize mRNA to myelin sheaths. However, insertion of the sequence motifs isolated from *fmr1* or *eif4ebp2* were not sufficient to localize mRNA to

myelin (Figure 7B,C). Together these data show that the sequences derived from the *mbpa* 3' UTR are necessary and sufficient for mRNA localization to myelin in vivo. These data suggest that these cis-regulatory elements and associated trans-acting factors are the minimal components necessary for mRNA localization. However, the sequences derived from *fmr1* and *eif4ebp2* are necessary but not sufficient for mRNA localization, indicating that additional molecular interactions within the 3' UTRs are important for 3' UTR-mediated localization of these transcripts.

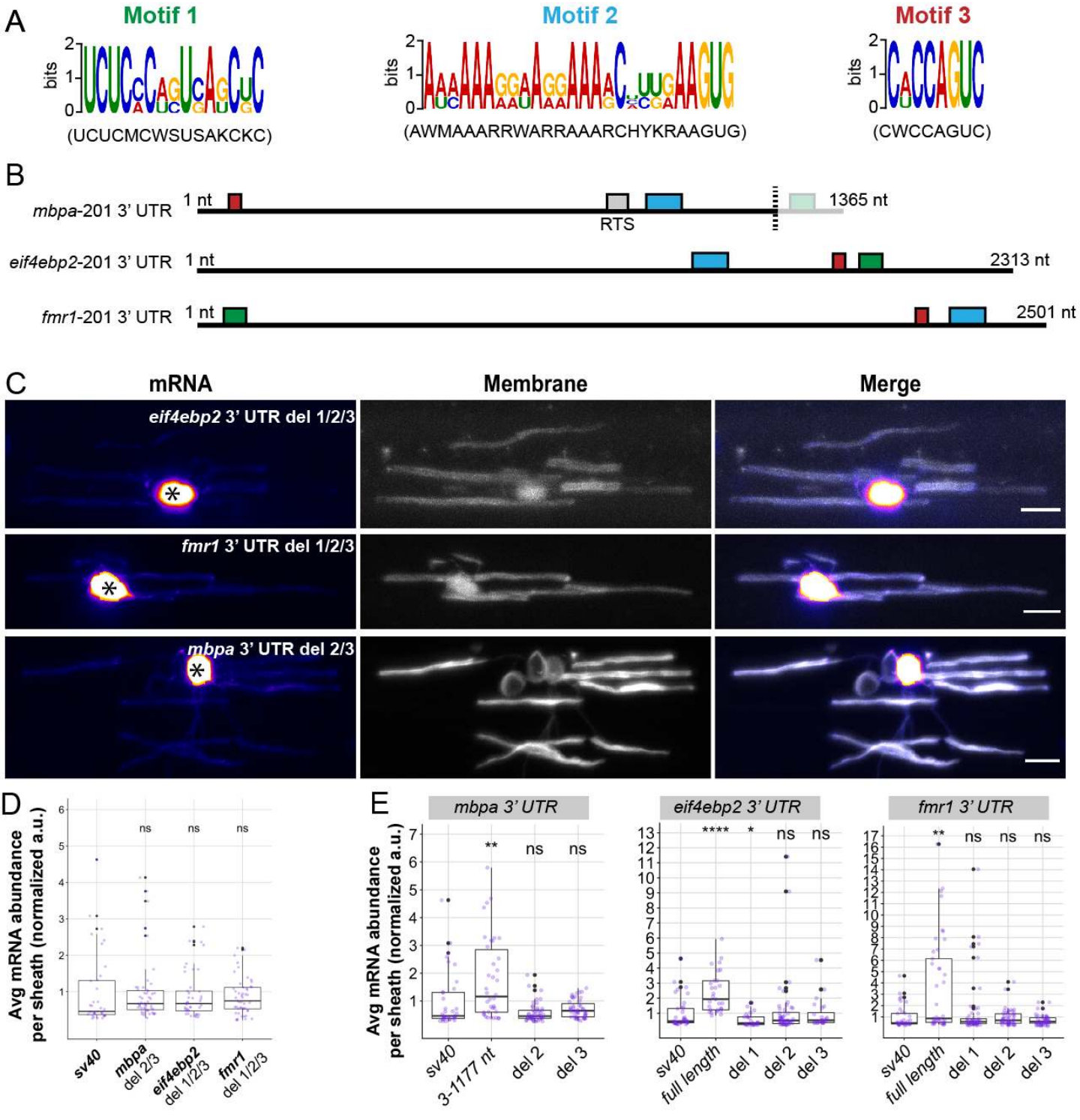

Figure 6. Common motifs in candidate 3' UTRs are required for myelin localization

(A) Schematic representation of the three motifs identified in the 3' UTRs of *mbpa-201*, *eif4ebp2-201,* and *fmr1-201* from the annotated zebrafish genome (GRCz11) using MEME suite bioinformatics software. (B) Schematic

representation of shared motifs within the 3' UTRs. Green box is motif 1, blue box is motif 2, red box is motif 3. Grey box is the conserved RTS previously identified as a minimal localization element necessary for *Mbp* mRNA transport in cultured oligodendrocytes (28,29,50). Motif 1 in the *mbpa* 3'UTR is not present in 3' UTR isolated from zebrafish cDNA utilized in experimental procedures (3' end of the dashed line). (C) Representative images of MS2 system after sequential deletions for all motifs from *mbpa*, *eif4ebp2*, and *fmr1* 3' UTRs. Asterisks mark cell bodies. (D) Quantification of mRNA abundance in myelin sheaths from sequential deletions. (E) Quantification of mRNA abundance in myelin sheaths from full length 3' UTR, *mbpa* 3' UTR variant 3-1177, or individual motif deletions. Statistical analysis evaluated with Wilcoxon test. Scale bars, 10 μm. A minimum (n) of 6 embryos and 35 sheaths were used in each condition (D-E).

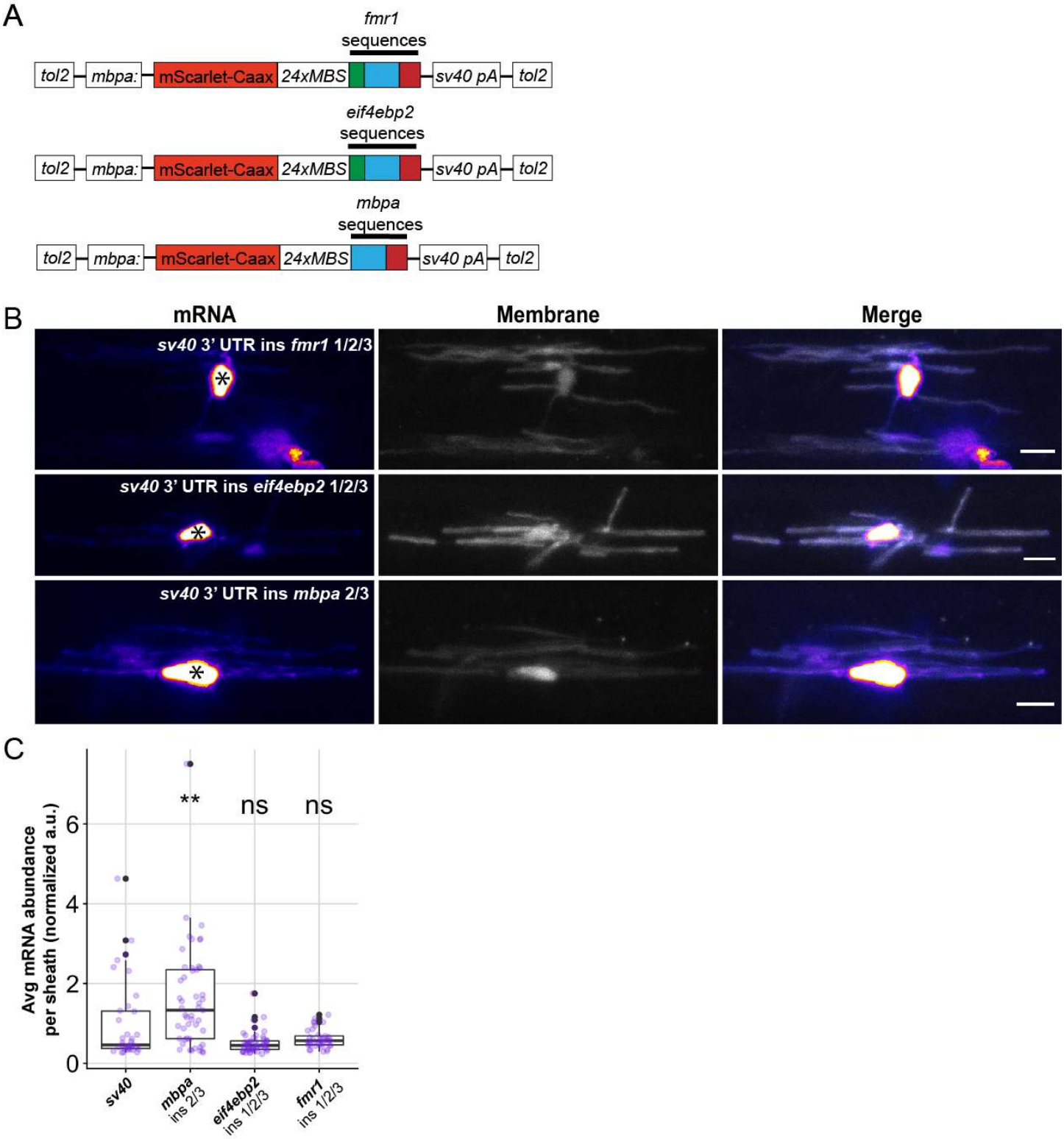

Figure 7. Sequence motifs derived from the *mbpa* 3' UTR are sufficient for mRNA localization to myelin

(A) Schematic representation of the MS2 mRNA reporter with motifs inserted upstream of the *sv40* 3'UTR. Green box is motif 1, blue box is motif 2, red box is motif 3. (B) Representative images of MS2 system after motifs from the *mbpa*, *eif4ebp2*, or *fmr1* 3' UTRs were inserted into the MS2 mRNA reporter. Asterisks mark cell bodies. (C)

Quantification of mRNA abundance in myelin sheaths from (B). Statistical analysis evaluated with Wilcoxon test. Scale bars, 10 μm. A minimum (n) of 6 embryos and 35 sheaths were used in each condition.

Localization motifs are enriched in the myelin transcriptome

Our analyses revealed motifs shared between localized transcripts. Are these motifs commonly found in the myelin transcriptome? We cross referenced myelin-localized transcripts with those from oligodendrocytes using two independent RNA-seq datasets to exclude non-oligodendrocyte transcripts (43,51). We identified 1855 transcripts localized to myelin (Supplemental Table 1) of which 1771 had significantly higher expression in the myelin transcriptome and were fully annotated in the genome browser. We found that motif 1 and 3 were not enriched in these transcripts compared to randomized, length-matched control sequences. However, motif 2 was significantly enriched in the 1771 transcripts of the myelin transcriptome (Figure 8A). Specifically, 42.4% (751 mRNAs) of myelin-localized transcripts contain one or more copies of motif 2 (Figure 8B, Supplemental Table 2). By comparison, we found that motif 2 is present at least once in only 28.7% of the mouse transcriptome (Figure 8C, Supplemental Table 3). Localization motifs are frequently positioned in the 3' UTRs of mRNA. We found that 63.8% of the motif 2 sites are positioned in the 3' UTRs of myelin-localized transcripts (Figure 8D, Supplemental Table 4-6). Together, these data suggest that motif 2 is a localization signal utilized by many transcripts for 3'UTR-mediated localization to myelin.

To determine if motif 2 is represented in particular subset of mRNAs within the myelin transcriptome, we performed gene ontology analysis on all myelin-localized transcripts as well as the subset of myelin-localized transcripts containing motif 2. Previous reports investigating the myelin transcriptome show enrichment of biological processes such as nervous system development, cellular respiration, and neurogenesis (27). Assessment of our 1771 myelin-localized genes was consistent with previous reports in that we also identified biological processes and cellular component terms pertaining to mitochondria, electron transport chain, and oxidative reduction. Importantly, we also identified GO terms associated with myelination such as myelin sheath, membrane, and protein

transport (Figure 8E, Supplemental Table 7). Next, we narrowed our gene list to the subset of myelin-localized transcripts that contain motif 2 (751 genes) to determine if these genes are functionally distinct. We identified biological mechanisms associated with synaptic signaling, nervous system development, and regulation of cellular projections. Interestingly, many of the genes are associated with cellular functions in distal projections such as postsynaptic density, synaptic vesicles, axon, dendrite, and terminal bouton (Figure 8F, Supplemental Table 8). Many of the biological functions are neuronal in nature with a remarkable lack of terms associated with myelination. These observations raise the possibility that nascent myelin sheaths engage in molecular mechanisms during axon wrapping that are similar to synaptogenic mechanisms. Overall, these findings implicate motif 2 as a regulatory element for a distinct cohort of transcripts within myelin sheaths.

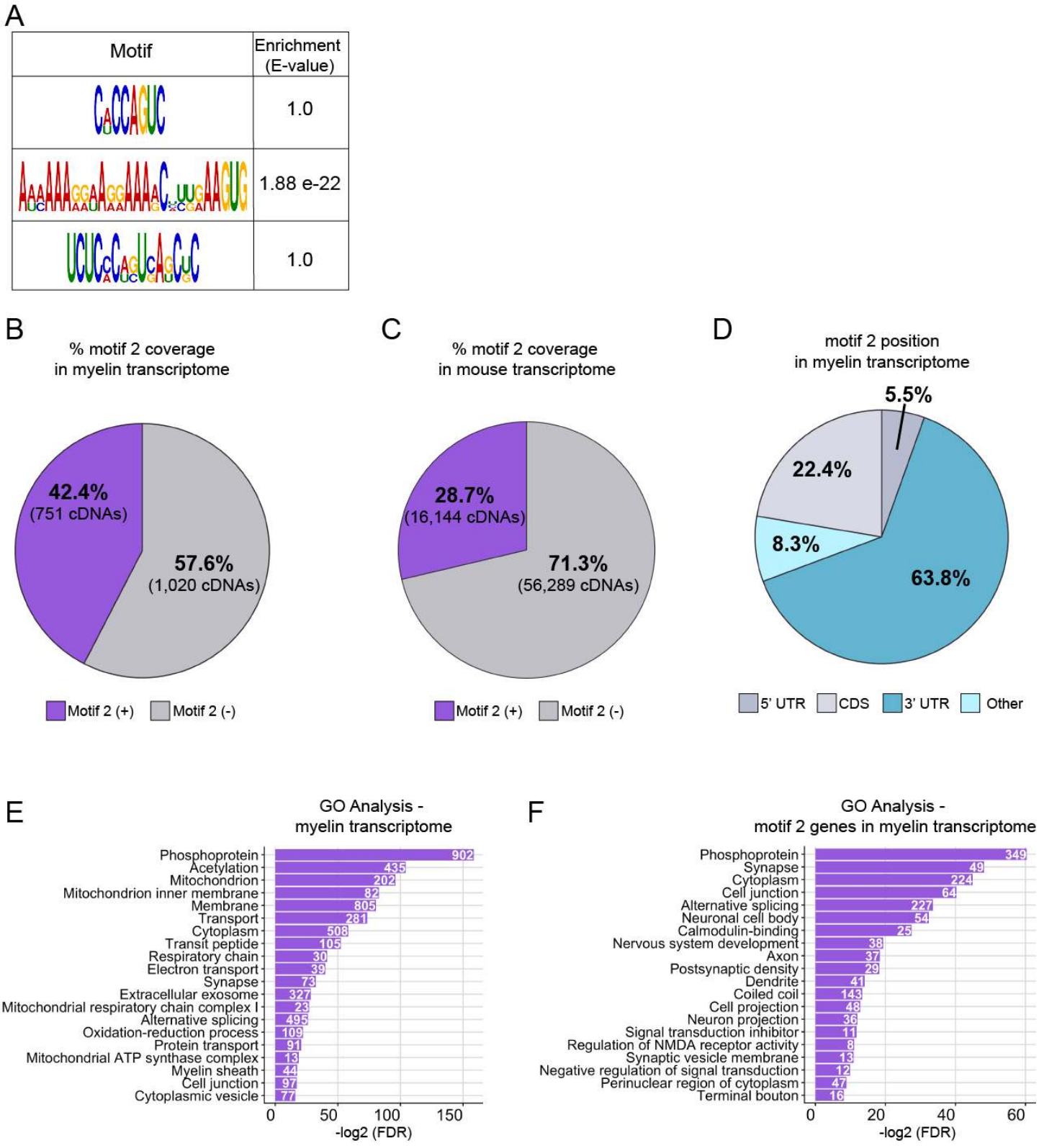

Figure 8. Motif 2 is enriched in the mouse myelin transcriptome

(A) Schematic representation of motif 1, 2, or 3 enrichment in the myelin transcriptome in comparison to length-matched, randomized sequences using MEME suite Analysis of Motif Enrichment (version 5.1.1) (52). (B) FIMO

(Find Individual Motif Occurrences version 5.1.1) was used to determine the frequency at which motif 2 is present in the myelin transcriptome (53). cDNA sequences from the myelin transcriptome were analyzed for the presence of motif 2. One or more copies of motif 2 were present in 42.4% of myelin cDNAs. (C) FIMO was used to determine the frequency at which motif 2 is present in the mouse transcriptome. cDNA sequences from the mouse annotated genome (mm10) were analyzed for the presence of motif 2. One or more copies of motif 2 were present in 28.7% of mouse cDNAs. (D) Percentage of motif 2 occurrences in 5' UTR, coding sequences, 3' UTR or other positions in myelin transcriptome. Motifs in the "other" category represent motifs overlapping two regions. (E) Top 20 gene ontology terms identified in the myelin transcriptome. (F) Top 20 gene ontology terms identified in myelin transcripts containing motif 2. Terms are ordered from most to least significant based on -log2 of the false discovery rates. Counts represent number of genes identified with the GO term.

DISCUSSION

The molecular mechanisms underlying myelin sheath growth are not well understood. Purified myelin contains hundreds of mRNAs (27), lending the possibility that mRNA localization and local translation promote sheath growth and maturation. How are mRNAs selectively targeted to myelin sheaths? Here we show that cis-regulatory elements found in candidate 3' UTRs are required for mRNA localization to myelin during ensheathment of target axons in vivo. In particular, one sequence is enriched in the myelin transcriptome implicating the motif as a potential regulator of mRNA localization in oligodendrocytes.

With high resolution microscopy we found *mbpa* mRNA concentrated near the growth zones of nascent myelin membrane. What accounts for enrichment near growth zones? For the last several decades, the mechanisms underlying *MBP* mRNA localization have been heavily investigated and revealed that transcripts are actively transported through oligodendrocyte processes to myelin sheaths in kinesin and dynein-dependent manners (36,54,55). Consistent with these data, recent work showed that microtubules are present in nascent sheaths in vivo (56). Nascent membrane also contains F-actin

which is specifically present in the leading edge (39,57). Importantly, actin-based transport can localize mRNA, mediated by myosin motor proteins (33,58,59) but this has yet to be tested in myelinating oligodendrocytes in vivo. Here we show that mRNA containing the *mbpa* 3' UTR is colocalized with F-actin in myelin sheaths. These observations raise the possibility that *Mbp* mRNA is handed off from microtubule-based transport to actin-based transport within growing sheaths.

Hundreds of mRNAs are localized to myelin, but it is unclear if these transcripts utilize 3'UTR-dependent localization mechanisms. Of the candidates we tested, four out of seven 3' UTRs were sufficient to drive mRNA into nascent sheaths. Thus, for some mRNAs, cis-regulatory elements important for mRNA localization might be embedded in 5' UTRs, coding regions, or retained introns of the transcripts (60–62). Alternatively, transcripts might occupy myelin by diffusion. Notably, we identified two transcripts that utilize their 3' UTRs for localization to myelin, *eif4ebp2* and *fmr1,* which encode translational regulators. Importantly, *fmr1* mRNA and the encoded protein, FMRP, have precedence for being localized to subcellular compartments, such as dendritic spines, far from the cell body (63). By finding mRNAs encoding translation regulators in myelin, our data support the possibility that transcripts encoding translational proteins are themselves locally translated within individual sheaths. In support of this model, purified myelin contains a free and polyribosome ribosome fraction (5), electron micrographs revealed ribosomes in the distal ends of oligodendrocyte processes (64) and a MBP reporter protein was translated in cultured oligodendrocyte precursor cells (Wake, Lee and Fields, 2011). Furthermore, our own work indicates that Fmrp (44) and Eif4ebp1 (unpublished) proteins are localized to nascent sheaths. This evidence raises the possibility that local protein synthesis of translational regulators may modulate localized protein expression within myelin sheaths. Testing this model directly will require methods for visualization of de novo translation in vivo (65–69).

The candidate 3' UTRs we selected were isolated from genes encoding cytosolic and transmembrane proteins. Canonically, transmembrane proteins are translated in the rough endoplasmic reticulum, processed by the golgi apparatus and transported via the secretory pathway. Identifying mRNAs encoding transmembrane proteins in the myelin transcriptome suggests that

noncanonical pathways regulate protein synthesis of transmembrane proteins in nascent sheaths. Consistent with this hypothesis, we found that the 3' UTR of *lrrtm1*, a transcript encoding a transmembrane protein, is sufficient to localize mRNA to nascent sheaths. In contrast, we found that the *cadm1b* 3' UTR is not sufficient to localize mRNA to myelin although we have previously show that the Cadm1b protein is present in myelin and regulates sheath length and number (41). Together, these observations raise the possibility that some transmembrane proteins are locally synthesized. In support of this hypothesis, distal oligodendrocyte processes contain satellite structures of rough endoplasmic reticulum (70). Future work will need to test the hypothesis that some transmembrane proteins undergo noncanonical synthesis near sites of sheath growth.

We identified cis-regulatory elements in the 3' UTRs of myelin-localized mRNAs. To begin, we bioinformatically identified three motifs common to the *mbpa*, *eif4ebp2*, and *fmr1* 3' UTRs. Each motif was necessary for localization, but only the sequences derived from the *mbpa* 3' UTR were sufficient to drive mRNA to nascent sheaths. However, we are not able to exclude the possibility the motif 1 in the *mbpa* 3' UTR contributes to mRNA localization. We interpret these data to mean that motifs 2 and 3 are minimal localization elements for *mbpa* 3' UTR-dependent localization in vivo. However, the sequences present in *eif4ebp2* and *fmr1* 3' UTRs, while necessary for localization, were not sufficient and thus require additional localization signals present in the 3' UTR, which are currently unknown. The capacity for motifs 2/3 to promote mRNA localization when isolated from the *mbpa* 3' UTR but not the *eif4ebp2* or *fmr1* 3' UTRs can be explained by two alternative possibilities. First, the primary sequences in the *mbpa* motifs are important for interacting with key trans-acting factors, such as RNA binding proteins, that are not able to interact with the primary sequences in the motifs from *eif4ebp2* and *fmr1* 3' UTRs. Second, the *mbpa* motifs form a secondary structure that is sufficient for myelin localization. Importantly, these alternative explanations may not be mutually exclusive and together demonstrate the complexities underlying mRNA sorting.

We found that motif 2 is enriched in the myelin transcriptome and approximately two-thirds of these motifs are positioned in the 3' UTRs, suggesting that motif 2 significantly contributes to mRNA localization in oligodendrocyte. To the best of our knowledge, motif 2 does not correspond to any known mRNA localization signals in oligodendrocytes. Gene ontology analysis of myelin-localized transcripts containing motif 2 indicates that many of these transcripts encode proteins with biological functions important in cellular and neural projections. Specifically, we identified genes associated with neuronal cellular compartments such as axon, dendrites, synapse, postsynaptic density, neuron projection, cell projection, synaptic vesicle membrane, and terminal bouton. These data support the model that myelin sheath growth utilizes molecular mechanisms similar to synaptogenesis (41). Together these data raise the possibility that motif 2 mediates localization of a cohort of mRNAs that encode proteins that function in distal ends of cellular projections, implicating the motif as a mRNA regulon. RNA regulons are primary sequences or secondary structures that are co-regulated at the post-transcriptional level to coordinate cellular functions (71–74). Identification of the trans-acting factors that interact with the motifs we identified will provide future insights into the molecular functions of myelin sheath growth, which will lead to a more complete understanding of the mechanisms guiding developmental myelination.

AUTHOR CONTRIBUTIONS

K.M.Y. and B.A. conceived the project. K.M.Y. performed all the experiments and collected and analyzed all the data. J.H.H. cloned the *mbpa* 3' UTR sequence and created *Tg(mbpa:EGFP-CAAX-polyA-CG2)*^{co53}. R.O. created the myelin transcriptome gene list and performed FIMO bioinformatics analysis to identify frequency of motifs in the myelin transcriptome. K.M.Y. and B.A. wrote the manuscript.

ACKNOWLEDGMENTS

We are grateful to Florence Marlow for her generous gift of the MS2 plasmids. We thank Karlie Fedder and Douglas Shepherd for their guidance during smFISH quantification. We thank Caleb Doll for comments on the manuscript. This work was supported by US National Institutes of Health (NIH) grant R01 NS095670 and a gift from the Gates Frontiers Fund to B.A. K.M.Y was supported by NIH (NIGMS) T32 fellowship GM008730, the Victor W. Bolie and Earleen D. Bolie Graduate Scholarship Fund, and as a RNA Scholar of the RNA Bioscience Initiative, University of Colorado School of Medicine. J.H.H was supported by a National Multiple Sclerosis Postdoctoral Fellowship (FG 2024-A-1) and NIH (NIMH) fellowship T32 MN015442. The University of Colorado Anschutz Medical Campus Zebrafish Core Facility was supported by NIH grant P30 NS048154. All DNA plasmids and transgenic zebrafish used in this study are available by request.

DECLARATION OF INTERESTS

The authors declare no competing financial interests.

STAR METHODS

CONTACT FOR REAGENT AND RESOURCE SHARING

Further information and requests for resources and reagents should be directed to and will be fulfilled by the Lead Contact, Bruce Appel (bruce.appel@ucdenver.edu).

EXPERIMENTAL MODEL AND SUBJECT DETAILS

Zebrafish lines and husbandry

All procedures were approved by the University of Colorado Anschutz Medical Campus Institutional Animal Care and Use Committee (IACUC) and performed to their standards. All non-transgenic embryos were obtained from pairwise crosses of male and females from the AB strain. Embryos were raised at 28.5°C in E3 media (5 mM NaCl, 0.17 mM KCl, 0.33 mM CaCl, 0.33 mM $MgSO_4$ at pH 7.4, with sodium bicarbonate) and sorted for good health and normal developmental patterns. Developmental stages are described in the results section for individual experiments.

The transgenic line *Tg(mbpa:EGFP-CAAX-polyA-CG2)*^{co34} was created by Dr. Jacob Hines. The transgenic construct was created using Gateway tol2 kit (Kwan et al 2007). Specifically, p5E-*mbpa* contains 2.6-kb genomic fragment of zebrafish *mbpa* (Hines et al. 2015). *pME-EGFP-CAAX*, *p3E-polyA* and *pDEST-tol2-CG2* were created by Dr. Jacob Hines. All entry vectors and destination were combined using LR clonase and transformed into DH5α cells. Colonies were screened by enzymatic digestion using BamHI, KpnI, and XhoI. Plasmid DNA was injected into AB embryos which were screened for transgenesis and outcrossed to create transgenic lines. All *Tg(mbpa:EGFP-CAAX-polyA-CG2)*^{co34} used in this manuscript were from F3 or later generations.

METHOD DETAILS

Candidate 3' UTR selection

To select 3' UTR candidates for cloning into the MS2 system we utilized published transcriptomics data (Thakurela et al. 2016). We downloaded Supplementary Table 1 containing transcript abundance in four stages of myelin development identified by RNA-sequencing. We selected the three biological replicates from P18 for analysis because this developmental timepoint was the most similar to our model. We filtered these data for transcripts with normalized read counts greater than 20 for all 3 biological replicates (representing 21,937 genes). We put all gene names into a gene ontology analysis (geneontology.org) and analyzed the genes for biological processes in Mus musculus. From these biological processes, we copied all genes into an Excel document that fit the term "synap", "translation", "myelin" and "oligodend". Biological terms identified in gene ontology analysis are listed in Table 1.

Table 1: List of Biological Process for GO Terms

"Synap"	**"Translation"**	**"Myelin"**	**"Oligodend"**
Regulation of Synaptic vesicle cycle	Translation	Regulation of Myelination	Oligodendrocyte Differentiation
Regulation of trans-synaptic signaling	Positive Regulation of Translation	Negative Regulation of Myelination	-
Synaptic Signaling	Regulation of Translation	Ensheathment of Neurons	-
Synaptic Plasticity	Negative Regulation of Translation	Paranode Assembly	-
Synaptic Vesicle Cycle	-	Myelin Assembly	-
Synaptic Vesicle Localization	-	Central Nervous System Myelination	-
Synapse Organization	-	-	-

Positive Regulation of Synaptic Transmission	-	-	-
Regulation of Synapse Structure or Activity	-	-	-

After removing duplicate genes with a GO term, the "Synap" list contained 855 genes, the "Translation" list contained 534 genes, the "myelin" list contained 128 genes and the "oligodend" list contained 28 genes. To further narrow our search, we cross-referenced these lists with one another to find genes that were common to more than one list, which resulted in 55 genes. To further narrow this list, we cross-referenced these genes with the Brain RNA Seq online database (Zhang et al. 2014) to identify those with evidence of oligodendrocyte lineage cell expression. We next referenced these genes with the zebrafish genome browser (GRCz11) and searched for annotated 3' UTRs for each. Finally, we performed literature searches for published data that were relevant to our model. This resulted in a final list of ten candidate 3' UTRs: *dlg1, cyfip1, eif4ebp2, fmr1, cadm1, lrrtm1, eif4g1, eif4a3, mtmr2* and *nfasc*.

3' UTR cloning

To clone the *mbpa 3' UTR*, 5 dpf cDNA from zebrafish larvae was used for PCR amplification using primers to target the flanking regions of the *mbpa* 3' UTR. The PCR fragment was cloned into pCR2.1 TOPO using the TOPO cloning kit. Colonies were screened by colony PCR. Using Gateway cloning, the *mbpa 3' UTR* was amplified and inserted into pDONR-P2R-P3 using BP clonase. *p3E-mbpa 3' UTR* was confirmed by sequencing. All cloning steps were performed by Dr. Jacob Hines.

To clone the additional full length 3' UTRs, cDNA was created from pooled 6 dpf AB larvae treated with 1 mL of Trizol and snap frozen. All RNA isolation steps were performed on ice and in a 4° centrifuge at 18,078 x g. Larvae were thawed on ice and homogenized with a 23 g needle. 200 µL of chloroform was added and shaken for 15 seconds followed by centrifugation for 10 min. The aqueous layer was transferred to a new tube and an equal volume of 100% cold isopropanol and 2 µL of glycogen blue was added to the sample. The tube was incubated at -20° for 20 min and centrifuged for 10 min. The supernatant was removed and transferred to a new tube and 200 µL of cold 70% ethanol was added to wash the pellet followed by 5 min centrifugation. This step was repeated. After the pellet dried, the RNA was resuspended in 20 µL of molecular grade water. RNA was quantified using a Nanodrop. To synthesize cDNA, we followed manufacturer instructions from the iScript™ Reverse Transcription Supermix for RT-qPCR, which uses random hexamer primers to synthesize cDNA.

To amplify the 3' UTRs from cDNA, we designed primers that flanked the annotated 3' UTR as predicted by *Danio rerio* GRCz11 annotated genome. Primers were flanked with attB sequences (Table 2) for cloning into the pDONR-P2R-P3 vector of the Tol2 Gateway kit (Kwan et al. 2007). cDNA was used as a PCR template to amplify the 3' UTRs. Of the ten 3' UTRs we attempted to amplify we were successful with the six listed below. Following amplification, bands were gel extracted using a Qiagen Gel Extraction Kit and cloned into pDONR-P2R-P3 using BP clonase. Clones were verified by sequencing using M13 forward and M13 reverse primers. The p3E-*dlg1* 3' UTR was not fully sequenced due to highly repetitive sequences. We sequenced approximately 51% of the construct from 1-54 and 775-1552 base pairs. We therefore confirmed p3E-*dlg1* 3' UTR identity using restriction enzyme mapping.

The *sv40* 3' UTR is a transcription termination and polyadenylation signal sequence isolated from Simian virus 40. We obtained this sequence from the Tol2 Gateway-compatible kit where it is referred to as "pA". This sequence was cloned with Gateway BP clonase into pDONR-P2R-P3. The p3E-sv40 3' UTR was confirmed by sequencing.

Table 2. Primers for UTR amplification and cloning

3' UTR name	Forward Primer (5'->3')	Reverse Primer (5'->3')	3' UTR Length (nt)	Percentage of annotated 3' UTR cloned
lrrtm1-201	ggggacagctttcttgtacaaagtggtatccacccatgtcagtttttacaaatcaatg	ggggacaactttgtataataaagttgttgttttccacttcaattgtgtctgttcg	368	93.6%
fmr1-201	ggggacagctttcttgtacaaagtggtaccttcccctcattctcccact	ggggacaactttgtataataaagttgtttgcagaggaagatcaacctttatttattgaaa	2486	99.4%
eif4ebp2-201	ggggacagctttcttgtacaaagtggtaagaagaggaacctacgtgaacaac	ggggacaactttgtataataaagttgtgtccactggcattggca	2282	98.5%
dlg1-201	ggggacagctttcttgtacaaagtggtaggggccgaagacaaataaacct	ggggacaactttgtataataaagttgtatggaatgaatcaagttggcagattatgtac	1522	97.2%
cyfip1-201	ggggacagctttcttgtacaaagtggtagcaccagtttgaagtggaagagat	ggggacaactttgtataataaagttgtaaaaaggcacgtttatgaggagtaagaac	585	88.1%
cadm1b-201	ggggacagctttcttgtacaaagtggtactggaactagacctgttagcttcc	ggggacaactttgtataataaagttgtcatttaaactgcttttattcactgttataatt	1220	100%
mbpa-201	gccttctccaagcaggaaaacactgagatg	gcagagtatatgagacacagaac	1174	86%

MS2 plasmid construction

All MS2 constructs were created using Gateway cloning. pME-*HA-NLS-tdMCP-EGFP* and pME-*24xMBS* were generous gifts from Dr. Florence Marlow.

To create pME-*mScarlet-CAAX-24xMBS*, we obtained plasmid pmScarlet_C1 from Addgene. In-Fusion™ cloning was used to assemble mScarlet-CAAX in puc19. Next, we amplified mScarlet-CAAX sequence using primers 5'-ggggacaagtttgtacaaaaaagcaggcttaatggtgagcaagggcgag-3' and 5'-ggggaccactttgtacaagaaagctgggtttcaggagagcacacacttgcag-3' and cloned it in plasmid pDONR-221 using BP clonase to create pME-mScarlet-CAAX. Next, we designed primers flanked with BamHI cut sites (5' -tccggatccatggtgagcaagggcgaggcag-3' and (5'-cgactctagaggatcgaaagctgggtcgaattcgcc-3') and PCR amplified the mScarlet-CAAX sequence. We purified the amplified product using QIAquick PCR Purification Kit and digested it with BamHI-HF. pME-*24xMBS* was linearized with BamHI-HF and treated with Antarctic phosphatase to prevent religation. We performed the ligation with 2X Quick Ligase and the ligation reaction was transformed into DH5α competent cells. Clones were screened using restriction mapping, then sequenced for confirmation.

For expression plasmids containing full length 3' UTRs, we used Gateway multi-site LR clonase to combine entry vectors with pDEST-tol2. The resulting expression plasmids included: pEXPR-*mbp:mScarlet-Caax-24xMBS-mbpa 3'UTR-tol2*, pEXPR-*mbpa:mScarlet-Caax-24xMBS-lrrtm1 3'UTR-tol2*, pEXPR-*mbpa:mScarlet-Caax-24xMBS-fmr1 3'UTR-tol2*, pEXPR-*mbpa:mScarlet-Caax-24xMBS-eif4ebp2 3'UTR-tol2*, pEXPR-*mbpa:mScarlet-Caax-24xMBS-dlg1 3'UTR-tol2*, pEXPR-*mbpa:mScarlet-Caax-24xMBS-cyfip1 3'UTR-tol2*, pEXPR-*mbpa:mScarlet-Caax-24xMBS-sv40 3'UTR-tol2* and pEXPR-*mbpa:mScarlet-Caax-24xMBS-cadm1b 3'UTR-tol2*. LR clonase reactions were transformed into Stellar Competent Cells (Takara cat # 636763). Clones were screened using restriction mapping.

To delete motifs, we used New England Biolabs Q5 Site Directed mutagenesis kit. Specifically, we designed primers flanking the motifs to omit the localization sequences from p3E-full length templates. We followed instructions outline in the kit to generate specific deletions. This step was repeated sequentially to delete all motifs from the previous template.

Table 3. Primers for motif deletions from full length 3' UTR

3' UTR name / motif ID	Forward Primer (5'->3')	Reverse Primer (5'->3')
mbpa / motif 2	caagatggataatgtggg	tcataccctttcctttatg
mbpa / motif 3	gcagcgagtttaacagac	agtctgtagggcagacatc
eif4ebp2 / motif 1	ttgtgcttagcctccgta	ggaaaaaataaatcattctgtgcc
eif4ebp2 / motif 2	ttgttttggtcatcgtac	ttgattatcaaggttcgtg
eif4ebp2 / motif 3	tttgtctgaggcacagaatg	cacagaaaaagacaattaaagtc
fmr1 / motif 1	caccaatccagatgcttc	atgaggggaaggtaccac

fmr1 / motif 2	ttgccaaacagactgttttc	ttttaacagactggtgaac
fmr1 / motif 3	tgttaaaaaaaaaaaaaaaaaaaaccttgaag	aactctgccatcttgcca

To insert motifs into a Gateway entry vector, we provided Genscript with Gateway entry vector pDONR-P2R-P3 and the sequences for each gene to be synthesized. Genscript synthesized the sequences and cloned them into the Gateway entry vector between the attR2 and attL3 sites. Motifs (underlined) were separated by 3-4 random nucleotides.

The sequences synthesized from *fmr1* motifs were 5'-ggagctctagtctcccactcagctcgcacaccagtcgataaaaaaaaaaaaaaaaccttgaagtgattc-3', from *eif4ebp2* motifs were 5'- ggagctctagatcaaaggtaggaaagcactgaagtggcactccagtcgattctcacagtgatctcattc-3', from *mbpa* motifs were 5'-ggagctctagcaccagtcgctcaaaaaaaggaaggaaaacctgaaagtggatattc-3'.

For control experiments to determine the specificity of mRNA detection by MCP-EGFP, we created an expression plasmid that lacks the 24xMBS stem loops (pEXPR-*mbpa:mScarlet-Caax-mbpa 3'UTR-tol2*).

Lifeact Cloning for F-actin reporter

The filamentous actin reporter was created using Gateway cloning. Alexandria Hughes created pME-lifeact-mNeonGreen by PCR amplification using primers 5'-ggggacaagtttgtacaaaaaagcaggctaccatgggcgtggccgacttga-3' and 5'-ggggaccactttgtacaagaaagctgggttcttgtacagctcgtccatgccca-3' from mNeonGreen-Lifeact-7. We then combined entry vectors and pDEST-tol2 using LR clonase to create pEXPR-*mbpa:lifeact-mNeonGreen-polyA-tol2*.

3' UTR sequences used for MS2 RNA localization experiments

Underlined sequences indicate the sequence motifs deleted or inserted in motif experiments.

sv40 3' UTR

5'-gatccagacatgataagatacattgatgagtttggacaaaccacaactagaatgcagtgaaaaaaatgctttatttgtgaaatttgtgatgctattgctttatttgtaaccatt

ataagctgcaataaacaagttaacaacaacaattgcattcattttatgtttcaggttcaggggggaggtgtgggaggtttttt -3'

mbpa 3' UTR

5’-

cttctccaagcaggaaaacactgagatggaagagagtgaaatggacggaaagcaaaaacttgagagggaggatgtctgccctacagact

caccagtcgcagcga

gtttaacagactaacattggccatcttcgcttcctagatagagatacaatccaagtatctgttgctacatgcctgcagggttacagaagcacgtgtt

gactgtatgtgtgcaaacttgctgtaataattgtcaatggtcaggtgatgcgatacatcttgtaagtctccctttaaaatttagctgaagtgatcaattt

caatatatacaaagagcaaaaactcatacaaaaggtttgaaacaattagacagagtatttctctttttttaaaatccctgaaccaaccagatgaa

tcatttgatcattctgaattggtcttatatgtgtttcacaaaatggattgcttatatgctctccagcatttgatgtgtggcatttattctatgttatactgcctct

ccatggttttcttgagatccatgttcaacctcatgtgatgtgcatttctgtatgtttgtgttcactgtggtctttgtgttgcattctatattggttatttactttata

ccaggaatttgtatataggaatctttattgagttttaattaatgcaaaaaaaaatatgatgaccagttaactacattaaatttgattcattttgagaaat

gatttagctcttaatcaggaccatgccttaaaatgattaaaaacagactaaaaacacaattttgtggactagggaatagattctaagcatgtatgt

ggcttggattgtatgccctcagatgttgcactgcagtatgtgtgttaaaaccacctgtaaatgttgtctgcgtcattacatgtgcaattttggtgttatttt

agaaaggtctcgtaattaccaggggtaggattaatatttaaataacaaacatgcagaaatctaggacaaagagtcagtgggagcataaagg

aaagggtatgaaaaaaaggaaggaaaacctgaaagtgcaagatggataatgtgggaaatgctaaatgaggacttctgaaagagtaaggt

ggagtttattcagctgatttttttttttcttttttctgtgttgtatctcatgtgtcttaatatcgttcattgttctgtgtctcatatactctgcc- 3’

eif4ebp2 3’ UTR

5’-

aagaagaggaacctacgtgaacaacgattaattacctggtacctgtgtgccagtggcttggcttgtagataccaatgttgtgagccctctccttta

gctctctctagctgctg

ggtgctgtttaatcatggggataaatgactaaagtttgcccagtggtgttgctggagccctgaaagttaacctgtgagccctgttgagctcttctttttt

gttgtttaggtttcagggctgccatcagcagtacttgcttgagtcacagagcaagggaaaaattctctattgcaagtgcccggatatattaccaatt

taccataatagactcataaacggatcagccattagagattcactgctgatagatcaaagtacactgttccagttgatgcccttaatgcagtctattt

cgttcacacataaactgatttgcaggacatgcggttatcattatctccctatattttcgattgtttttcccccagttaattttaaaagggacaacaggatt

atattcatatttttttgattcaaaaagtgaaaaaattccaatcattcctgctcttttatatcatttttttttttcacctcaatacatttttcaggtgttcaaaagaa

tagttttatattgttgtccaaaaatgcataattaaaccattgaccttaatcattcatttgaactgacacatgatttcaatgccaaatgtgcacagaattt

ctcattttatttaggactaccccaaaataagcatttcaggtcatattagtttaatttcccagttttttcactgttaattttaagaaaagaaacacctaatc

acattcgtgaaagaccaaactgttactttagattaaagagaatgtttctgttcagatttatttttgctaacagtaaggtttgtttctttgtttgtctttgagag

atgaagcgtcaacatagcctagttaaaagttaataacaccaagtaatgtttgattggataaagggtttaatataccttataagatgttgacaaaga

aagctggtctcaggaagcacttgctttatgcacctaacaattacgcatcttacggctcctgttacgggagaaaaagcacggtgaatatttaacatt

aatatcagctgtgacatctgctgttactttccgaaatactacaatcctcacgaaccttgataatcaaatcaaaggtaggaaagcactgaagtgtt

gttttggtcatcgtaccatcggtctgtctcataagcgcacacaatgtgaacgagttttgtcgcgagcagacattcattttgattcagatcaaacgtct

cgaaaacttgaattgaatctttccaatgctcttctatgcatgttctttcggtctgcttcttaagctttagttcacatgtcagatcattttaacgttgttgttttttg

ggggggggacgccaaatcgtgtggaagacgagaattattattgtaagagaattaagcaaagagattattcaaacaaagtgacttaaagagga

taagacttattctcatgactttaattgtctttttctgtgctccagtctttgtctgaggcacagaatgatttatttttttcctctcacagtgatctcttgtgcttagc

ctccgtatccatgccttactttactaagctgagcagctgtgtcaaatacagtacccttcataccttaaaacgggatcagttccttttctttcgtttctttca
agtggagaacaagatcaagatattgctgttttactagaaaacatttatatttttggagacatgtttgttatcatttactttcttacagaaatgggacgatt
tggaaatgcagaggtgtaatatttgtaatagtaatggattggttaaaagcaaatacagaatttaggtttgactttgaggtcacagttaagtttctattc
aattttgagaacttgtagaatccttggagtatgttttcatgtccggtttgcgcaaaagtcacattcaagttctaatgatttacagtgaagggaaattgg
tgtatactgtccttctgtaatggatatgaatggtcaaattccagcttgtttcaactctaaaattatgaaatgttaaatttttttatttaaaaaaaaataatg
cttactattgctttatgctttccccacgcatcaaactatcagaaatgcatttagttctgtgtgaggggatttaagatggacgtgttttatctaatatggca
aaaaacattggaaactgtattttctttcttctttgaccctgttaattttaatgaaatgccaatgccagtggacac- 3’

lrrtm1 3’ UTR

5’-

tccacccatgtcagtttttacaaatcaatgtacgggtggatatggaacatacgttaacttggcacccaattttgctgctctcaaagggagctacagt
tctggagtgtgagtgg

actacaaacatggatttagagctgatttcaacagcctcatggggaaatctgactgtgagacccgtgcacttgatgcaaaagatgtggaatgatt
atgctgaccagtcctggcttctcttgtgaaaagtggatatttgagctttaacgtgtctttctacttcaggatattctaggactctctaaagctaccgagg
acatcaagtacaccatggtaacaaacatacgaacagacacaattgaagtggaaaacaacaa- 3’

fmr1 3’ UTR

5’-

ccttcccctcattctcccactcagctccaccaatccagatgcttcttcattagagacacattaggccaaagagaaccaggtcagtagggctgtcg
caagacatgacata

aagcacactttgtaattgttagcggggttaaaagacaaggtctcttggtgtacggtgtgttgaatttggtagtcttcacggattagagagaccggtc
tctaaatctcaactgaagctacaggttttctaattgactttctaaataactacctaaagaagctgtggataaaatgtctctcataaatggaataaaa
acaaaaaaaagagcttttccaagaaattggtttttaaagtttgttttccacaatgtccaaaaaaaagggaaagaaacgcatcggaggatgaac
tcaagctctcgacgcccaagtttatgccacatctcatggcatacattgtttttacacgctttggtgtccatggtttctcgagcccattctgatgtgagat
cttaaccacatcattagcaaaaaaatacaaaaaaaaatttaaaaaacgaagagaaaaaataagtaaaaaataaaaaaaatgctcctgtctg
gatctgtgcctttaactagtgtggatagtatcataatttggatgtttaaatcagggaagaaggcgtgaacaacacctgtcacctgagcagagtttg
ttgcaatctcagccgacaactttaaaaacaaacaaaaaaaggtgtttctttttttttctctgtgctgcatgtatttcacaaacattttgtatgtctgaaaa
gcaggattggaaatctattttgccatagctgagttgtgagtagtaaaggtattagcctaactaaactagtcaactgtggaagtcattgattgtaact
aaccacccgagttgaatatcaatgctaattcaacaatgaaagcattaatgaagattaatttgatgtaaagcatatctttgcattttagaacaattgtt
ttttgttttcaatagaggtagcaaagcagtttcctttaaacaaaatgtcttttgttttttacttgttttacctccatcatgatataaaggtgaatttgctcaga
tgttttctcacaaacagggtggaaatgctctattttgtttcatttttttttttttgttcatgctggccacagtaaactgccatctttcctgctgtatttttcagcatc
aggtgtgaagcacttatatcagattatatctgtaacattgtctttgtcctaacaatggctcatcatagactgaaaatgttgaactgtgggattgcatac
tgtatattattacatcatccgttaagagattgttgctgttctttttagattgaactttaaatgtgcacttatcatgtttgtgttactctgcaagtactttataatc
tataaacctataataaactagaatgtgataagacttcttcagcaggtgaatcacatgtatgctgtcaacataactaaactgaagtttagatctcttc
gctaattttgagtctactgtacttttgcagcttcgagagggacgagatttgggggaaacacaacgttaactttgatatgaggagaacaaaatgtct
atcttatccgattagtgcttgtgcattaaactttagtttacaattttgagaagacgcaaagctgttctaaacccacgattcttttgaaacctactgtgac

ggtaaacatggtagttttttgactgtacagcaagaaagccagtcagttgtatcctctttgctccttttttcttaacaactctttttcattttatgctcgctagt
caaatatccagctctacctgtaaagcttacaccagtttcaaagtgattttgccttgatcagtgtcctgtgaaaaccaaacggaaggggttacgtttc
acgcgaaatgcaaaaaaaacctgtgactggcagaggatttgcagctctgtgggatgggaatgataaaccactcgaacggggcgtcctggct
gcatccggccccctttaaaatttagcctttatttggaagtaaggtgttaaaatggtttactcccagtatttttaaaaaaacttgcacatctacggtgtg
cagtaaactggcaagatggcagagttcaccagtctgttaaaaaaaaaaaaaaaaaaccttgaagtgttgccaaacagactgttttctagt
tatttatttttttggaatgtatatgaaaaatgacaaattgtaaaaccatctcttgcacacatcgttaggctattgtgatttgaataaagagctgaaaagg
aataaaaacaaacaaaaaacatgaaatactgtagatactgaaccgaggtagactgaccttgtatgttactgcactttgggtgataatttctttgta
cataatagcagaacagactgggttttatgttgacattgtttggttatagtgcaatatattttgtatgcaagcagtttcaataaataaaggttgatcttcct
ctgcaa- 3’

dlg1 3’ UTR

Note: dlg1 3’ UTR contains a region of thymidine repeats that inhibited sequencing a 35 bp region (nucleotides 7-41). Within the 35 bp region, 5 nucleotides were not able to be confirmed and are underlined in the sequence below. Together, we confirmed 99.7% of the dlg1 3’ UTR sequence used in experimental procedures.

5’-

ggggccgaagacaaataaaccttacacttctttaacttttgtatttttttttaatcttttcgtttccttttttaatattaacatggcctgcagcttgcattgg
ctttccaactcctgagcataagaaatgcgttttctttgaatgggtttggggtttttcctctttctctcatgcctctctttgaaactactgtctagaactcgca
tcccaatctccgcatgtggtcctccactgggaggagacgtgcttgaccagcgacttactggacagattatacggtacagattccttaatgtttaag
ggaggtgactttctcgaaggaaaaccaataagttaatgcattatacacattttggtttgttcttcatttttttacccccccagtatatgatcagaagcttt
catgtctgtctctggaaagacataaagcaaaactttgcacgtttttttgcatgtttggattattctgtttcagttaacatattgttcttacgtttttatgtcaga
cagatttaaaccatgtgactttcagccaccatatgactttagttttcttctaaaatcaagcaacccgttcactttatgcagctgatctgtttttgtcgcca
gtacacaaagaggatgataaaaaatttaatatttggcacaaaagttcttctttttatattaaatgtctatttgtcttaacgatctgtgtacattttaattaa
ggtgcatctgggagtagcttttagcagaggaacgggcttacgattatatttcaaacccagggtgacgacatattcttacttcaaaaaaacagca
atgcaaataagagagtataaattgtaatgtatattcaaccctcagtatactgcctattttgttataatgaaagtcctatattgagctttaattaaactct
acacctatgggaattattttctttataatgtcaagcatacactcgaatgactatgcgtgtatgtatataaaataaatataaatagatatatatttttttcct
ttacttttaccaccatcacttttgttgtttctggtttgtctttatgcaaaaacactgacacacacacgcacactaggctggatggtggatttccatttgca
tctgctccaacaatatgaaaacaaaactcaagttggcagtttgtagtattcagctctctctttgtctctctctcctgtgtaattctgtcatattttctttctca
tgtgacgtgcatgatttcttaaagcaatagtcttcatcagcaaggagcggaggagagggatttggcataaactgtaaacctgaaaggctgtatg
ggaattgttgaatgcccgtagctgaagagagatttgctttgcctttaactgtccaccaggggtgctgacggcatccccgctattttgttttctttcgttt
tttaactcggagatgattgttttctaaaagattgcttctctaacttgtcatcatggctttctaacacattttgactagataatgtacataatctgccaactt
gattcattccat- 3’

cyfip1 3’ UTR

5’-

gcaccagtttgaagtggaagagatgggaaaagagagggaaatatttagcaacgtgtttaggaccagtttcactgtcacattctacttaatgatg

ccttttcttatgccaccct
gtagtttctgcagagccagtaagttgccttgtgattggtcgagtgatttgatttgcaccaattactgcaccctactcaggctttggttaatcaggccaa
gatatgtttatgatgtacacaaacatggctcagttttactagcgtatttcaggttgatttttttttgtacacataaacacacacatacacacacactcgt
gccttattatagataaattgactataatcttttatatgttaatgatagcacagcactactcatgttttatacttgggaacagcagtggggtatggttcca
aaatggccaagtgggttttatcaaagggttatttaagcttttgctgtagtgcgagtccagcggtatttttttctatgtggtgttgaatgattgcatgcaagt
ttttttttcttctattatacttaataaaactttaagcgtagccaagttcttactcctcataaacgtgccttttt- 3’

cadm1b 3’ UTR

5’-
actggaactagacctgttagcttccagtgctgaacagcaaactgtggactgctgggtttgggaggaaggggttgtgggattcaatcaggctgga
ttcacacctgcgcag
ctgaagagacgctgctgccatcgagacggacggggtgtgggatggcagagcactaggagagctcaattttagaccgcttcaccatccaaca
cctcctgctggggccggttttgttccgtttaaacatttgctaagaattttgtgccttgttctgttcttactgaagttcccactttcatcaggacacccacaa
gctactgtctctccaatggtctgaatccacgttttttttttctctcctttcatttcatttttttaattgctagcacatcttaaagctctctctcatgctgttctgtctg
caggtctgaaagaaagccgcgcaccaagtttcgatgtaagattcagtcacagaatgatcgcttgggttgttttcacggattgattccaagtaatttt
atttggcaaattgcctgttgctctccttagtcccccagagaacgagttagagatgatagaaacctttttttctctctctttttttgtgaccaacaacattca
gcagcagtattgcattgttgcaatatttattggatatactgtatgcgattatgatcagcttgtgttgatattagggctgtcaatcgaacacattactact
attatttcgtttattaaatcattaaaatattacccaaatttggcaatgacatgacaaaatttatattattattattattatatacagctatggaaaaaatat
taagactaattatgacatttcttactaaattaaaatgaaaaagttattatttagagcattgttttttttttttgcttgtttgtttttttctttaaaaaaaaaggtgct
aaattttcagacatgttgctagccaaattcatttatatagaacatttcataaacagtaataattccaagtgctttacataaacaggaataaaagaa
acaagtataagaaaataaaaaacaaattataacagtgaataaaagcagtttaaaatg- 3’

smFISH probe design

The *EGFP* smFISH probes were purchased from Stellaris LGC Biosearch Technologies. Probes consist of a set of pooled oligos with CAL Fluor® Red 610 Dye. smFISH probes were designed using the Stellaris RNA FISH Probe Designer tool by entering the zebrafish *mbpa*, *eif4ebp2*, or *fmr1* cDNA sequences obtained from Ensemble Genome Browser from transcript *mbpa-206*, *eif4ebp2-201*, and *fmr1-201* (GRCz11) (Table 4-6). Probes with highly repetitive sequences were removed. Each probe was entered into BLAST to search for off targets and were removed if they were predicted to bind annotated genes with relatively high specificity. The probes were ordered with a CAL Fluor® Red 610 Dye. Probes were resuspended in Tris-EDTA, pH 8.0 and stored at a stock concentration of 12.5 µM at -20°C.

Table 4: Probe sequences for *mbpa-206*

Probe Name	Sequence 5'->3'	Probe Name	Sequence 5'->3'
Probe 1	ctttggattgagcggagaag	Probe 13	aatcttcaacctgggagaaa
Probe 2	gtccagactgtagaccactg	Probe 14	gatctcgctctccacccaaa
Probe 3	cagatcaacacctagaatgg	Probe 15	ctggagcaccatcttctgag
Probe 4	ctctggacaaaacccttcg	Probe 16	cttctccaagcaggaaaaca
Probe 5	tgtcctggatcaaatcagca	Probe 17	gagatggaagagagtgaaat
Probe 6	ttcttcggaggagacaagaa	Probe 18	cgggaagcaaaaacttgaga
Probe 7	agagaccccaccactctt	Probe 19	atgtctgccctacagactca
Probe 8	tcgtgcatttcttcaggagc	Probe 20	gtcgcagcgagtttaacaga
Probe 9	tcgtgcatttcttcaggagc	Probe 21	acattggccatcttcgcttc
Probe 10	tcgaggtggagagaactatt	Probe 22	agatagagatacaatccaag
Probe 11	cattagatcgccacagagac	Probe 23	tctgttgctacatgcctgca
Probe 12	aagggaacagaacacacttt	Probe 24	ttacagaagcacgtgttgac

Table 5: Probe sequences for *eif4ebp2-201*

Probe Name	Sequence 5'->3'	Probe Name	Sequence 5'->3'
Probe 1	ggaaagcgataagaaacgag	Probe 16	gcttggcttgtagataccaa
Probe 2	gaaagggcccgaggttttta	Probe 17	gccctctcctttagctctct
Probe 3	ttccatcggggaaaacttat	Probe 18	gctgggtgctgtttaatcat
Probe 4	agcaagtgcaatgtcgtcca	Probe 19	aaagtttgcccagtggtgtt
Probe 5	cgtcagcttagtgagagcag	Probe 20	gagccctgaaagttaacctg
Probe 6	ctgatcaacgactcaacgca	Probe 21	agccctgttgagctcttctt
Probe 7	ctcacgactattgcaccact	Probe 22	gcagtacttgcttgagtcac
Probe 8	tggaggcactttattctcca	Probe 23	agcaagggaaaaattctcta
Probe 9	gaggaacccgaataatctat	Probe 24	tgcccggatatattaccaat
Probe 10	tcgtaagttcctgttggacc	Probe 25	tgcccggatatattaccaat
Probe 11	gaatgaaatcaagcggaatg	Probe 26	tgatgcccttaatgcagtct
Probe 12	catcaacaaccatgatgcca	Probe 27	aaactgatttgcaggacatg
Probe 13	caaggtgaagatgctcagtt		
Probe 14	agatggacatctaaagaaga		
Probe 15	aacctacgtgaacaacgatt		

Table 6: Probe sequences for *fmr1-201*

Probe Name	Sequence 5'->3'	Probe Name	Sequence 5'->3'
Probe 1	ggagctttctacaaggctta	Probe 18	tgatctcgatgaagagacat

Probe 2	cagccagaacgacagatttc	Probe 19	tttcacatctatggagagga
Probe 3	tccaggatgttcggtttcca	Probe 20	ccgaagctacctggaatttt
Probe 4	tccaaccggttttcagaaag	Probe 21	aaaagtcattggcaagagtg
Probe 5	taatgataaggaaccctgtg	Probe 22	agctgattcaagaggttgtg
Probe 6	caaagttcgcatggtgaaag	Probe 23	taaatcgggtgttgtcagag
Probe 7	acgttatagaatatgcagcc	Probe 24	aaggagagcatttctaatgc
Probe 8	tgatgccaccctaaatgaaa	Probe 25	tattctgctggactaccatc
Probe 9	gtcacattagagaggctacg	Probe 26	tttaaaggaggtagatcagc
Probe 10	agcaacaaagaacacctttc	Probe 27	acccgagaaagaaaagtctt
Probe 11	aaaaccagactagatgttcc	Probe 28	caaacctttggtcgaggag
Probe 12	agacttgagacagatgtgtg	Probe 29	gagtctatgggttatcccaa
Probe 13	ctctgaagaaaagcagttgg	Probe 30	gatacaaaactgaggacatg
Probe 14	atccatgttgagtgacatgc	Probe 31	gtagttccagagactccaag
Probe 15	tttaggagtctgcgcacaaa	Probe 32	catcgacagcaataacgaga
Probe 16	tcatgaacagtttgtggtgc	Probe 33	gtagtgaacggcgtttcgta
Probe 17	aagccagaaagatttctgga		

smFISH experimental procedure

The smFISH protocol was adapted from three published protocols: Hauptmann and Gerster (2000), Lyubimova et al. (2013) and Oka et al (2015). First, larvae were sorted for EGFP expression and fixed O/N in 4% paraformaldehyde at 4°C. Larvae were embedded laterally in 1.5% agar, 5% sucrose blocks and transferred to a 30% sucrose solution O/N at 4°C. Blocks were frozen on dry ice and sectioned with a Leica cryostat into 20 µm thick sections and placed on microscope slides. Slides were not allowed to dry more than 5 min before adding 4% paraformaldehyde to fix the tissue at RT for 10-20 min. The slides were quickly rinsed with 1X PBS twice. The tissue was permeabilized with 70% cold ethanol at -20^{0}C for 2 hours. Parafilm was placed over tissue to prevent evaporation at all incubation steps. The tissue was rehydrated with wash buffer (10% DI formamide, 2X SSC in molecular grade water) for 5 min at RT. From this point on, care was taken to protect the tissue and probes from light as much as possible. Hybridization Buffer was made: 2x SSC, 10% DI formamide, 25mg/mL tRNA, 50mg/mL bovine serum albumin, 200mM ribonucleoside vanadyl complex in DEPC water. Aliquots were made and stored at -20^{0}C. Final probe concentrations for egfp and mbpa was 125nM. Final probe concentrations for eif4ebp2 and fmr1 was 250nM. Slides were incubated at 37^{0}C overnight in probe. Slides were quickly rinsed with fresh wash buffer followed by 2 wash steps at 37^{0}C for 30 minutes. DAPI was added at 1:1000 concentration in wash buffer to the tissue for 5-7 min at RT. Slides were quickly rinsed twice with wash buffer. Finally, slides were mounted with Vectashield mounting media and a No. 1 coverslip and sealed with nail polish. All slides were stored and protected from light at 4^{0}C.

Microscopy

To image RNA localization in living animals, plasmids were injected with mRNA encoding Tol2 transposase into newly fertilized eggs. Injection solutions contained 5 µL 0.4 M KCl, 250 ng Tol2 mRNA and 125 ng pEXPR-*sox10:NLS-tdMCP-EGFP-sv40 3' UTR-tol2* plasmid and 125 ng pEXPR-*mbpa:mScarlet-CAAX-various 3' UTR-polyA-tol2*. Larvae were grown to 4 dpf and selected for good health and normal developmental patterns. Larvae were immobilized in 0.6% low-melt agarose with 0.06% tricaine. Images of single timepoint data were obtained using a Zeiss LSM 880 laser scanning confocal microscope equipped with a 40x, 1.3 NA oil immersion objective. Imaging was performed using Zeiss Zen Black software with the following parameters: 1024 x 1024 frame size, 1.03 µsec pixel dwell time, 16-bit depth, 10% 488 laser power, 14% 561 laser power, 700 digital gain, 488 filter range 481-571, mScarlet filter range 605-695 and z intervals of 0.5 µm. All images of single cells were taken in the spinal cord of living zebrafish above the yolk extension. Cells were selected for imaging based on dual expression of EGFP and mScarlet-CAAX.

Images of smFISH experiments were obtained using a Zeiss LSM 880 with Airyscan confocal microscope and a Plan-Apochromat 63x, 1.4 NA oil immersion objective. The acquisition light path used Diode 405, Argon 488, HeNe 594 lasers, 405 beam splitter and 488/594 beam splitters, and Airyscan super resolution detector. Imaging was performed using Zeiss Zen Black software and parameters included: 1024 x 1024 frame size, 1.03usec pixel dwell time, 16-bit depth, 3x zoom. Line averaging was set to 2, 2-5% 488 laser power, 2% 594 laser power, 0.5-3% 405 laser power, 750 gain, and z intervals of 0.3 µm. All images of single cells were taken in the hindbrain of zebrafish larvae. Cells were selected for imaging based on expression of EGFP-CAAX and Quasar-610 fluorescence. Post-image processing was performed using Airyscan Processing set to 6.8 for images that were quantified. For representative images of *fmr1* and *eif4ebp2* smFISH, post-acquisition processing was performed using auto Airyscan Processing.

QUANTIFICATION AND STATISTICAL ANALYSIS

Quantification of MS2 RNA localization

All images were processed and analyzed using ImageJ Fiji software. To analyze mRNA fluorescent intensity in sheath termini, we imaged single cells co-expressing NLS-MCP-EGFP and mScarlet-CAAX. Individual myelin sheaths were optically isolated by performing a maximum z projection of images collected at 0.5 µm intervals. Fluorescence intensity was measured by performing line scans across a

7 μm (± 0.3 μm) distance beginning at the terminal end of each sheath. Specifically, we drew each line in the mScarlet-CAAX channel to ensure we encompassed the edge of the myelin membrane. Gray values along each line (at 0.2 μm intervals) were measured in both channels. All measurements were combined into a Microsoft Excel file and imported into RStudio for further processing and analysis. In RStudio we used tidyverse and ggplot2 libraries to manipulate data and generate plots. To normalize fluorescence intensities in each sheath, we divided the raw gray value at each distance by the average gray values of all distances per sheath. To calculate the average mRNA fluorescence intensity among all myelin sheaths, we plotted the average normalized fluorescence intensity by distance. To calculate mRNA fluorescence intensities in myelin sheaths, we plotted the average fluorescent intensity of EGFP (raw gray values) for each sheath using the line scan measurements described above.

To measure mRNA fluorescent intensity in cell bodies, we imaged single cells co-expressing NLS-MCP-EGFP and mScarlet-CAAX. Due to the high expression levels of EGFP in the nucleus, the 488 laser power was lowered to 0.3 to ensure we captured the full dynamic range of EGFP intensities. Cells containing saturated pixels were not utilized. During post-acquisition analysis, cell bodies were optically isolated by performing maximum z projection of images collected at 0.5 μm intervals. Fluorescence intensity was measured by drawing three regions of interest at the cell periphery, cell center, and between the periphery and center. Each region of interest was 3 pixels by 3 pixels. All data points were combined in Microsoft Excel and imported into RStudio for analysis. To calculate the average fluorescence intensity per cell, we averaged the three ROIs per cell. We normalized the intensity from each cell body to the average of all cell bodies in the *sv40* 3' UTR control.

smFISH Quantification

All quantification was performed in ImageJ Fiji using a custom script created by Karlie Fedder (available upon request). First, z intervals were selected for individual cells or myelin tracts using the "Make Substack" feature in Fiji. Substacks for cell bodies included all z intervals for each soma. Substacks of myelin tracts in the hindbrain included 100 pixel x 100 pixels and 13 steps with an interval of 0.3 μm (4.39 μm x 4.39 μm x 3.9 μm). This volume was chosen because it was approximately the same volume as cell bodies. Each substack was maximum z-projected. Background was subtracted using a 2.5 rolling ball. The image was then thresholded by taking 3 standard deviations above the mean fluorescence intensity. Puncta were analyzed using the "Analyze Particles" feature with a size of 0.01-Infinity and circularity of 0.00-1.00. Using the maximum projection of the EGFP-CAAX channel, a region of interest (ROI) was drawn around each cell body using the freehand tool. Alternatively, for myelin ROIs, the rectangle tool was used to draw a square 100 x 100 pixels (4.39 μm x 4.39 μm). All

thresholded puncta were inspected to ensure single molecules were selected. Occasionally, threshold puncta fell on the border of the ROI and these were excluded from measurements. *mbpa* transcripts are highly expressed and counting individual puncta was not consistently reliable. Therefore, to measure each puncta, we overlaid the binary image on the maximum z projected image and calculated the density (area x average fluorescence intensity) using the "IntDen" measurement.

To obtain the average mRNA abundance per subcellular compartment, we calculated the average density for all puncta in each ROI (cell bodies or myelin). All ROIs for each subcellular compartment were then averaged to calculate the average density per subcellular compartment.

Statistics

All statistics were performed in RStudio (version 1.1.456) using devtools (version 2.2.1) and ggplot2(Wickham 2009) packages. Additionally several packages and libraries were installed including tidyverse (Wickham et al. 2019), readxl (version 1.3.1), RColorBrewer (version 1.1-2), ggsignif (version 0.6.0), and ggpubr (version 0.2.4). All statistically analyses were performed with ggpubr. Wilcoxon rank sum was performed for unpaired comparisons of two groups.

BIOINFORMATIC ANALYSIS

Identifying Transcripts in the Myelin Transcriptome

To identify cDNA sequences in the myelin transcriptome associated with Supplemental Table 1 in the main text, we started with the myelin transcriptome obtained from Thakurela et al. (2016, Scientific Reports). Specifically, we used the data from the three biological replicates from P18 mice and these biological replicates were called "Treatment". As a control group, we used six RNA-seq datasets from two independent studies using cultured oligodendrocytes to eliminate any axonal-derived mRNAs (Marques et al. 2016 Science; Zhang et al. 2014 J Neurosci). Specifically, we used P7B2 and P7B3 datasets from Marques et al. and the 2 NFO and 2 MO datasets from Zhang et al. These datasets were called "Control" in Supplemental Table 1. We calculated the average abundance (FPKM) in the treatment group and control group and determined the fold change. Next, we filtered the data for transcripts that have a q-value less than 0.05. Finally, to eliminate any genes with low mRNA abundance (FPKM), we filtered the data to only include genes that have FPKM greater than 5 in the control or treatment groups.

MEME Analysis

To identify motifs shared between the *mbpa-201*, *eif4ebp2-201*, and *fmr1-201* 3' UTRs we used Multiple Em for Motif Elicitation (MEME) (version 5.1.1) part of the MEME suite software. We used the

default settings: Classic mode, RNA sequences, Zero or One Occurrence Per Sequence, and set the maximum motif to identify at 20 motifs. We selected the top 3 motifs for experimental procedures.

AME Analysis

To identify if motifs enriched in the myelin transcriptome, we used Analysis of Motif Enrichment (AME) (version 5.1.1) part of MEME suite software. Specifically, we downloaded cDNA sequences in fasta formats for transcripts present in the myelin transcriptome (1771 cDNA fasta sequences associated with the 1855 genes in Supplemental Table 1). Some genes had multiple cDNA sequences that correlate to splice variants and we selected the longest variant for our analysis. We uploaded these sequences into AME software and used the default settings to determine if motif 1, 2, or 3 were enriched in the myelin transcriptome. As a control sequence, we used shuffled input sequences.

FIMO Analysis

To determine the frequency of motif 2 occurrences in the various datasets, we used Find Individual Motif Occurrences (FIMO) (version 5.1.1) part of the MEME suite software. Specifically, we downloaded cDNA sequences from the entire mouse transcriptome (mm10), cDNA sequences from the myelin transcriptome, 5' UTR sequences from the myelin transcriptome, 3' UTR sequences from the myelin transcriptome, or coding sequences from the myelin transcriptome. We uploaded the sequences in to FIMO software and used the default settings to determine the number of occurrences for motif 2. Table 7 indicates the number of input sequences for each condition, number of occurrences motif 2 was identified, and the number of unique genes with one or more copies of motif 2. The results from each of these analyses can be found in the Supplemental Tables.

Table 7. FIMO Analysis results

Sequence Type	Number of Input Sequences	Number of Motif 2 Occurrences Found	Number of Unique Genes with Motif 2
cDNA from mouse transcriptome	56,289	36,662	16,144
cDNA from myelin transcriptome	1771	2101	751
5' UTRs from myelin transcriptome	1195	115	59
Coding sequences from myelin transcriptome	1411	470	751
3' UTR from myelin transcriptome	1404	1341	480

GO Analysis

To identify gene ontology terms associated with the myelin transcriptome and motif 2-containing myelin transcriptome, we used DAVID software (version 6.8). Specifically, we submitted Ensemble Gene IDs

from the myelin transcriptome (2821 genes) or the 751 genes containing motif 2. We selected GO term categories for biological processes, cellular compartment and up_keywords. We filtered the results for false discovery rate less than 0.05. We identified 60 terms in the myelin transcriptome and 34 terms in the motif 2-containing myelin transcriptome. We sorted the GO terms from lowest to highest FDR, removed any duplicate GO terms and selected the top 20 terms.

REFERENCES

1. Murtie JC, Macklin WB, Corfas G. Morphometric analysis of oligodendrocytes in the adult mouse frontal cortex. J Neurosci Res [Internet]. 2007 Aug 1 [cited 2019 Apr 2];85:2080–6. Available from: http://doi.wiley.com/10.1002/jnr.21339

2. Almeida RG, Czopka T, ffrench-Constant C, Lyons DA. Individual axons regulate the myelinating potential of single oligodendrocytes in vivo. Development. 2011 Oct 15;138(20):4443–50.

3. Chong SYC, Rosenberg SS, Fancy SPJ, Zhao C, Shen Y-AA, Hahn AT, et al. Neurite outgrowth inhibitor Nogo-A establishes spatial segregation and extent of oligodendrocyte myelination. Proc Natl Acad Sci U S A [Internet]. 2012 Jan 24 [cited 2019 Apr 18];109(4):1299–304. Available from: http://www.ncbi.nlm.nih.gov/pubmed/22160722

4. de Vries H, Schrage C, Hoekstra D. An Apical-Type Trafficking Pathway Is Present in Cultured Oligodendrocytes but the Sphingolipid-enriched Myelin Membrane Is the Target of a Basolateral-Type Pathway. Mol Biol Cell [Internet]. 1998 Mar [cited 2019 Dec 19];9(3):599–609. Available from: https://www.molbiolcell.org/doi/10.1091/mbc.9.3.599

5. Colman DR. Synthesis and incorporation of myelin polypeptides into CNS myelin. J Cell Biol [Internet]. 1982 Nov 1;95(2):598–608. Available from: http://www.jcb.org/cgi/doi/10.1083/jcb.95.2.598

6. Schwob VS, Clark HB, Agrawal D, Agrawal HC. Electron Microscopic Immunocytochemical Localization of Myelin Proteolipid Protein and Myelin Basic Protein to Oligodendrocytes in Rat Brain During Myelination. J Neurochem [Internet]. 1985 Aug 1 [cited 2020 Feb 24];45(2):559–71. Available from: http://doi.wiley.com/10.1111/j.1471-4159.1985.tb04024.x

7. Ainger K, Avossa D, Morgan F, Hill SJ, Barry C, Barbarese E, et al. Transport and localization of exogenous myelin basic protein mRNA microinjected into oligodendrocytes. J Cell Biol. 1993;123(2):431–41.

8. Kristensson K, Zeller NK, Dubois-dalcq ME, Lazzarini RA. The Journal of Histochemistry Expression of Myelin Basic Protein Gene in the Developing Rat Brain as Revealed by in Situ Hybridization. J Histochem Cytochem [Internet]. 1986 [cited 2019 Apr 2];34(4):467–73. Available from: https://journals.sagepub.com/doi/pdf/10.1177/34.4.2419396

9. Trapp BD, Moench T, Pulley M, Barbosa E, Tennekoon G, Griffin J. Spatial segregation of mRNA encoding myelin-specific proteins (oligodendrocytes/Schwann cells/in situ hybridization/immunocytochemistry). Neurobiology [Internet]. 1987 [cited 2018 Dec 26];84:7773–7. Available from: https://www.pnas.org/content/pnas/84/21/7773.full.pdf

10. Wake H, Lee PR, Fields RD. Control of Local Protein Synthesis and Initial Events in Myelination by Action Potentials. Science (80-) [Internet]. 2011;333(6049):1647–51. Available from: http://www.sciencemag.org/cgi/doi/10.1126/science.1206998

11. Minis A, Dahary D, Manor O, Leshkowitz D, Pilpel Y, Yaron A. Subcellular transcriptomics-Dissection of the mRNA composition in the axonal compartment of sensory neurons. Dev Neurobiol [Internet]. 2014 Mar 1 [cited 2019 Mar 18];74(3):365–81. Available from: http://doi.wiley.com/10.1002/dneu.22140

12. Briese M, Saal L, Appenzeller S, Moradi M, Baluapuri A, Sendtner M. Whole transcriptome profiling reveals the RNA content of motor axons. Nucleic Acids Res [Internet]. 2016 Feb 29 [cited 2019 Mar 18];44(4):e33–e33. Available from: https://academic.oup.com/nar/article-lookup/doi/10.1093/nar/gkv1027

13. Taylor AM, Berchtold NC, Perreau VM, Tu CH, Li Jeon N, Cotman CW. Axonal mRNA in uninjured and regenerating cortical mammalian axons. J Neurosci [Internet]. 2009 Apr 15 [cited 2019 May 6];29(15):4697–707. Available from: http://www.ncbi.nlm.nih.gov/pubmed/19369540

14. Cajigas IJ, Tushev G, Will TJ, Tom Dieck S, Fuerst N, Schuman EM. The Local Transcriptome in the Synaptic Neuropil Revealed by Deep Sequencing and High-Resolution Imaging. Neuron [Internet]. 2012

[cited 2018 Sep 20];74(3):453–66. Available from: https://www.ncbi.nlm.nih.gov/pmc/articles/PMC3627340/pdf/emss-52755.pdf

15. Zivraj KH, Chun Y, Tung L, Piper M, Gumy L, Fawcett JW, et al. Cellular/Molecular Subcellular Profiling Reveals Distinct and Developmentally Regulated Repertoire of Growth Cone mRNAs. 2010 [cited 2018 Sep 17]; Available from: www.jneurosci.org

16. Huber KM, Kayser MS, Bear MF. Role for rapid dendritic protein synthesis in hippocampal mGluR-dependent long-term depression. Science [Internet]. 2000 May 19 [cited 2018 Dec 14];288(5469):1254–7. Available from: http://www.ncbi.nlm.nih.gov/pubmed/10818003

17. Zhang X hui, Poo M. Localized synaptic potentiation by BDNF requires local protein synthesis in the developing axon. Neuron [Internet]. 2002 Nov 14 [cited 2019 Mar 18];36(4):675–88. Available from: http://www.ncbi.nlm.nih.gov/pubmed/12441056

18. Kang H, Schuman EM. A Requirement for Local Protein Synthesis in Neurotrophin-Induced Hippocampal Synaptic Plasticity. Science (80-). 1996;273(5280):1402–6.

19. Leung K-M, Holt CE. Live visualization of protein synthesis in axonal growth cones by microinjection of photoconvertible Kaede into Xenopus embryos. Nat Protoc [Internet]. 2008 [cited 2017 Oct 3];3(8):1318–27. Available from: http://www.ncbi.nlm.nih.gov/pubmed/18714300

20. Taliaferro JM, Vidaki M, Oliveira R, Gertler FB, Swanson MS, Burge Correspondence CB, et al. Distal Alternative Last Exons Localize mRNAs to Neural Projections. Mol Cell [Internet]. 2016 [cited 2018 May 3];61:821–33. Available from: http://dx.doi.org/10.1016/j.molcel.2016.01.020

21. Tushev G, Glock C, Heumüller M, Biever A, Jovanovic M, Schuman EM. Alternative 3' UTRs Modify the Localization, Regulatory Potential, Stability, and Plasticity of mRNAs in Neuronal Compartments. Neuron. 2018;98(3):495-511.e6.

22. Zhang HL, Eom T, Oleynikov Y, Shenoy SM, Liebelt DA, Dictenberg JB, et al. Neurotrophin-Induced Transport of a β-Actin mRNP Complex Increases β-Actin Levels and Stimulates Growth Cone Motility. Neuron [Internet]. 2001 Aug 2 [cited 2019 Apr 3];31(2):261–75. Available from:

https://www.sciencedirect.com/science/article/pii/S0896627301003579?via%3Dihub

23. Kislauskis EH, Zhu X, Singer RH. Sequences responsible for intracellular localization of β-actin messenger RNA also affect cell phenotype. J Cell Biol. 1994 Oct 15;127(2):441–51.

24. Bassell GJ, Zhang H, Byrd AL, Femino AM, Singer RH, Taneja KL, et al. Sorting of β-actin mRNA and protein to neurites and growth cones in culture. J Neurosci. 1998;18(1):251–65.

25. Welshhans K, Bassell GJ. Netrin-1-induced local β-actin synthesis and growth cone guidance requires zipcode binding protein 1. J Neurosci. 2011 Jul 6;31(27):9800–13.

26. Donnelly CJ, Willis DE, Xu M, Tep C, Jiang C, Yoo S, et al. Limited availability of ZBP1 restricts axonal mRNA localization and nerve regeneration capacity. EMBO J [Internet]. 2011 Nov 16 [cited 2020 Apr 30];30(22):4665–77. Available from: http://emboj.embopress.org/cgi/doi/10.1038/emboj.2011.347

27. Thakurela S, Garding A, Jung RB, Müller C, Goebbels S, White R, et al. The transcriptome of mouse central nervous system myelin. Sci Rep [Internet]. 2016;6(1):25828. Available from: http://www.nature.com/articles/srep25828

28. Ainger K, Avossa D, Diana AS, Barry C, Barbarese E, Carson JH. Transport and localization elements in myelin basic protein mRNA. J Cell Biol. 1997;138(5):1077–87.

29. Torvund-Jensen J, Steengaard J, Askebjerg LB, Kjaer-Sorensen K, Laursen LS. The 3'UTRs of Myelin Basic Protein mRNAs Regulate Transport, Local Translation and Sensitivity to Neuronal Activity in Zebrafish. Front Mol Neurosci. 2018;11:185.

30. Munro TP, Magee RJ, Kidd GJ, Carson JH, Barbarese E, Smith LM, et al. Mutational analysis of a heterogeneous nuclear ribonucleoprotein A2 response element for RNA trafficking. J Biol Chem [Internet]. 1999 Nov 26 [cited 2019 Apr 18];274(48):34389–95. Available from: http://www.ncbi.nlm.nih.gov/pubmed/10567417

31. Hoek KS, Kidd GJ, Carson JH, Smith R. hnRNP A2 Selectively Binds the Cytoplasmic Transport Sequence of Myelin Basic Protein mRNA † [Internet]. 1998 [cited 2019 Apr 18]. Available from: https://pubs.acs.org/sharingguidelines

32. Holz A, Schaeren-Wiemers N, Schaefer C, Pott U, Colello RJ, Schwab ME. Molecular and developmental characterization of novel cDNAs of the myelin-associated/oligodendrocytic basic protein. J Neurosci. 1996 Jan 15;16(2):467–77.

33. Bertrand E, Chartrand P, Schaefer M, Shenoy SM, Singer RH, Long RM. Localization of ASH1 mRNA Particles in Living Yeast. Mol Cell [Internet]. 1998 Oct 1 [cited 2019 May 6];2(4):437–45. Available from: https://www.sciencedirect.com/science/article/pii/S1097276500801434?via%3Dihub

34. Fitzgerald M, Shenk T. THE SITE AT WHICH LATE mRNAs ARE POLYADENYLATED IS ALTERED IN SV40 MUTANT dl882. Ann N Y Acad Sci [Internet]. 1980 Nov 1 [cited 2019 May 24];354(1 Genetic Varia):53–9. Available from: http://doi.wiley.com/10.1111/j.1749-6632.1980.tb27957.x

35. Buj R, Iglesias N, Planas AM, Santalucía T. A plasmid toolkit for cloning chimeric cDNAs encoding customized fusion proteins into any Gateway destination expression vector. BMC Mol Biol [Internet]. 2013 Aug 20 [cited 2019 Apr 6];14(18):1–16. Available from: http://bmcmolbiol.biomedcentral.com/articles/10.1186/1471-2199-14-18

36. Lyons D a, Naylor SG, Scholze A, Talbot WS. Kif1b is essential for mRNA localization in oligodendrocytes and development of myelinated axons. Nat Genet [Internet]. 2009;41(7):854–8. Available from: http://dx.doi.org/10.1038/ng.376%5Cnhttp://www.ncbi.nlm.nih.gov/pubmed/19503091%5Cnhttp://www.nature.com.ezproxy.library.ubc.ca/ng/journal/v41/n7/full/ng.376.html

37. Herbert AL, Fu M, Drerup CM, Gray RS, Harty BL, Ackerman SD, et al. Dynein/dynactin is necessary for anterograde transport ofMbpmRNA in oligodendrocytes and for myelination in vivo. Proc Natl Acad Sci. 2017;114(43):E9153–62.

38. Snaidero N, Möbius W, Czopka T, Hekking LHP, Mathisen C, Verkleij D, et al. Myelin Membrane Wrapping of CNS Axons by PI(3,4,5)P3-Dependent Polarized Growth at the Inner Tongue. Cell [Internet]. 2014 Jan;156(1–2):277–90. Available from: https://linkinghub.elsevier.com/retrieve/pii/S0092867413015304

39. Nawaz S, Sánchez P, Schmitt S, Snaidero N, Mitkovski M, Velte C, et al. Actin Filament Turnover Drives

Leading Edge Growth during Myelin Sheath Formation in the Central Nervous System. Dev Cell [Internet]. 2015 Jul 27 [cited 2018 May 16];34(2):139–51. Available from: http://www.ncbi.nlm.nih.gov/pubmed/26166299

40. Zuchero JB, Fu M-M, Sloan SA, Soderling SH, Miller RH, Barres Correspondence BA, et al. CNS Myelin Wrapping Is Driven by Actin Disassembly. DEVCEL [Internet]. 2015 [cited 2018 May 31];34:152–67. Available from: http://dx.doi.org/10.1016/j.devcel.2015.06.011

41. Hughes AN, Appel B. Oligodendrocytes express synaptic proteins that modulate myelin sheath formation. Nat Commun [Internet]. 2019 Dec 11 [cited 2019 Sep 16];10(1):4125. Available from: http://www.nature.com/articles/s41467-019-12059-y

42. Ravanelli AM, Kearns CA, Powers RK, Wang Y, Hines JH, Donaldson MJ, et al. Sequential specification of oligodendrocyte lineage cells by distinct levels of Hedgehog and Notch signaling. Dev Biol [Internet]. 2018 Dec 15 [cited 2019 Jan 18];444(2):93–106. Available from: https://www.sciencedirect.com/science/article/pii/S0012160618304755?via%3Dihub

43. Zhang Y, Chen K, Sloan SA, Bennett ML, Scholze AR, O'Keeffe S, et al. An RNA-Sequencing Transcriptome and Splicing Database of Glia, Neurons, and Vascular Cells of the Cerebral Cortex. J Neurosci [Internet]. 2014 Sep 3;34(36):11929–47. Available from: http://www.jneurosci.org/cgi/doi/10.1523/JNEUROSCI.1860-14.2014

44. Doll CA, Yergert KM, Appel BH. The RNA binding protein fragile X mental retardation protein promotes myelin sheath growth. Glia [Internet]. 2020 Mar 18 [cited 2020 Jan 19];68(3):495–508. Available from: https://onlinelibrary.wiley.com/doi/abs/10.1002/glia.23731

45. D'Hooge R, Nagels G, Franck F, Bakker CE, Reyniers E, Storm K, et al. Mildly impaired water maze performance in male Fmr1 knockout mice. Neuroscience. 1997 Jan;76(2):367–76.

46. Banko JL, Poulin F, Hou L, DeMaria CT, Sonenberg N, Klann E. The translation repressor 4E-BP2 is critical for eIF4F complex formation, synaptic plasticity, and memory in the hippocampus. J Neurosci [Internet]. 2005 Oct 19 [cited 2019 May 15];25(42):9581–90. Available from: http://www.ncbi.nlm.nih.gov/pubmed/16237163

47. Van Dam D, D'Hooge R, Hauben E, Reyniers E, Gantois I, Bakker CE, et al. Spatial learning, contextual fear conditioning and conditioned emotional response in Fmr1 knockout mice. Behav Brain Res. 2000 Dec 20;117(1–2):127–36.

48. Bailey TL, Boden M, Buske FA, Frith M, Grant CE, Clementi L, et al. MEME SUITE: tools for motif discovery and searching. Nucleic Acids Res [Internet]. 2009 Jul 1 [cited 2020 Jan 28];37(Web Server):W202–8. Available from: https://academic.oup.com/nar/article-lookup/doi/10.1093/nar/gkp335

49. Bailey T, Elkan C. Fitting a mixture model by expectation maximization to discover motifs in biopolymers. In: Proceedings of the Second International Conference on Intelligent Systems for Molecular Biology. AAAI Press; 1994. p. 28–36.

50. Brosamle C, Halpern ME. Characterization of Myelination in the Developing Zebrafish. Glia [Internet]. 2002 [cited 2020 May 14];39:47–57. Available from: http://workbench.sdsc.edu/

51. Marques S, Zeisel A, Codeluppi S, van Bruggen D, Mendanha Falcão A, Xiao L, et al. Oligodendrocyte heterogeneity in the mouse juvenile and adult central nervous system. Science [Internet]. 2016 Jun 10 [cited 2017 Nov 1];352(6291):1326–9. Available from: http://www.ncbi.nlm.nih.gov/pubmed/27284195

52. McLeay RC, Bailey TL. Motif Enrichment Analysis: a unified framework and an evaluation on ChIP data. BMC Bioinformatics [Internet]. 2010 Dec 1 [cited 2020 Feb 11];11(1):165. Available from: https://bmcbioinformatics.biomedcentral.com/articles/10.1186/1471-2105-11-165

53. Grant CE, Bailey TL, Noble WS. FIMO: scanning for occurrences of a given motif. Bioinformatics [Internet]. 2011 Apr 1 [cited 2020 Feb 11];27(7):1017–8. Available from: https://academic.oup.com/bioinformatics/article-lookup/doi/10.1093/bioinformatics/btr064

54. Carson JH, Worboys K, Ainger K, Barbarese E. Translocation of myelin basic protein mRNA in oligodendrocytes requires microtubules and kinesin. Cell Motil Cytoskeleton. 1997;38(4):318–28.

55. Herbert AL, Fu M-M, Drerup CM, Gray RS, Harty BL, Ackerman SD, et al. Dynein/dynactin is necessary for anterograde transport of Mbp mRNA in oligodendrocytes and for myelination in vivo. Proc Natl Acad Sci U S A. 2017;114(43):E9153–62.

40 56. Fu M, McAlear TS, Nguyen H, Oses-Prieto JA, Valenzuela A, Shi RD, et al. The Golgi Outpost Protein
41 TPPP Nucleates Microtubules and Is Critical for Myelination. Cell [Internet]. 2019 Sep;179(1):132-
42 146.e14. Available from: https://linkinghub.elsevier.com/retrieve/pii/S0092867419309134

43 57. Zuchero JB, Fu M-M, Sloan SA, Ibrahim A, Olson A, Zaremba A, et al. CNS myelin wrapping is driven
44 by actin disassembly-supplement. Dev Cell [Internet]. 2015 Jul 27 [cited 2018 May 31];34(2):152–67.
45 Available from: http://www.ncbi.nlm.nih.gov/pubmed/26166300

46 58. Yoshimura A, Fujii R, Watanabe Y, Okabe S, Fukui K, Takumi T. Myosin-Va facilitates the accumulation
47 of mRNA/protein complex in dendritic spines. Curr Biol [Internet]. 2006 Dec 5 [cited 2018 Oct
48 31];16(23):2345–51. Available from: http://www.ncbi.nlm.nih.gov/pubmed/17141617

49 59. Krauss J, López de Quinto S, Nüsslein-Volhard C, Ephrussi A. Myosin-V Regulates oskar mRNA
50 Localization in the Drosophila Oocyte. Curr Biol [Internet]. 2009 Jun 23 [cited 2019 May 8];19(12):1058–
51 63. Available from: https://www.sciencedirect.com/science/article/pii/S0960982209011178?via%3Dihub

52 60. Buckley PT, Lee MT, Sul JY, Miyashiro KY, Bell TJ, Fisher SA, et al. Cytoplasmic Intron Sequence-
53 Retaining Transcripts Can Be Dendritically Targeted via ID Element Retrotransposons. Neuron. 2011
54 Mar 10;69(5):877–84.

55 61. Hachet O, Ephrussi A. Splicing of oskar RNA in the nucleus is coupled to its cytoplasmic localization.
56 Nature [Internet]. 2004 Apr 29 [cited 2020 Feb 20];428(6986):959–63. Available from:
57 http://www.nature.com/articles/nature02521

58 62. Meer EJ, Wang DO, Kim S, Barr I, Guo F, Martin KC. Identification of a cis-acting element that localizes
59 mRNA to synapses. [cited 2020 Feb 20]; Available from:
60 www.pnas.org/cgi/doi/10.1073/pnas.1116269109

61 63. Antar LN, Afroz R, Dictenberg JB, Carroll RC, Bassell GJ. Metabotropic Glutamate Receptor Activation
62 Regulates Fragile X Mental Retardation Protein and Fmr1 mRNA Localization Differentially in Dendrites
63 and at Synapses. J Neurosci. 2004 Mar 17;24(11):2648–55.

64 64. Lunn KF, Baas PW, Duncan ID. Microtubule Organization and Stability in the Oligodendrocyte. J

Neurosci [Internet]. 1997 [cited 2017 Apr 27];17(13):4921–32. Available from: http://www.jneurosci.org/content/jneuro/17/13/4921.full.pdf

65. Halstead JM, Lionnet T, Wilbertz JH, Wippich F, Ephrussi A, Singer RH, et al. An RNA biosensor for imaging the first round of translation from single cells to living animals. Science [Internet]. 2015 Mar 20 [cited 2017 Oct 3];347(6228):1367–671. Available from: http://www.ncbi.nlm.nih.gov/pubmed/25792328

66. Yan X, Hoek TA, Vale RD, Tanenbaum ME. Dynamics of Translation of Single mRNA Molecules In Vivo. Cell [Internet]. 2016 May 5 [cited 2019 Jan 28];165(4):976–89. Available from: http://www.ncbi.nlm.nih.gov/pubmed/27153498

67. Morisaki T, Lyon K, DeLuca KF, DeLuca JG, English BP, Zhang Z, et al. Real-time quantification of single RNA translation dynamics in living cells. Science [Internet]. 2016 Jun 17 [cited 2019 May 8];352(6292):1425–9. Available from: http://www.ncbi.nlm.nih.gov/pubmed/27313040

68. Wang C, Han B, Zhou R, Zhuang X. Real-Time Imaging of Translation on Single mRNA Transcripts in Live Cells. Cell [Internet]. 2016 May 5 [cited 2019 May 8];165(4):990–1001. Available from: https://www.sciencedirect.com/science/article/pii/S0092867416304834

69. Pichon X, Bastide A, Safieddine A, Chouaib R, Samacoits A, Basyuk E, et al. Visualization of single endogenous polysomes reveals the dynamics of translation in live human cells. J Cell Biol [Internet]. 2016 Sep 12 [cited 2019 May 8];214(6):769–81. Available from: http://www.ncbi.nlm.nih.gov/pubmed/27597760

70. Waxman SG, Sims TJ. Specificity in central myelination: evidence for local regulation of myelin thickness. Brain Res [Internet]. 1984 Jan 30 [cited 2018 Jun 14];292(1):179–85. Available from: https://www.sciencedirect.com/science/article/pii/0006899384909053?via%3Dihub

71. Tenenbaum SA, Carson CC, Lager PJ, Keene JD. Identifying mRNA subsets in messenger ribonucleoprotein complexes by using cDNA arrays. Proc Natl Acad Sci U S A. 2000 Dec 19;97(26):14085–90.

72. Hogan DJ, Riordan DP, Gerber AP, Herschlag D, Brown PO. Diverse RNA-Binding Proteins Interact

with Functionally Related Sets of RNAs, Suggesting an Extensive Regulatory System. Sean R. Eddy, editor. PLoS Biol [Internet]. 2008 Oct 28 [cited 2020 Feb 5];6(10):e255. Available from: https://dx.plos.org/10.1371/journal.pbio.0060255

73. Narla A, Ebert BL. Ribosomopathies: human disorders of ribosome dysfunction. Blood [Internet]. 2010 [cited 2017 Jul 20];115(16). Available from: http://www.bloodjournal.org/content/115/16/3196?sso-checked=true

74. Culjkovic-Kraljacic B, Borden KLB. The Impact of Post-transcriptional Control: Better Living Through RNA Regulons. Front Genet. 2018 Nov 5;9.